

Final Technical Report

Project Title: Optimization of a Virtual Power Plant to Provide Frequency Support

Project Period: 10/1/14 – 11/30/15

Submission Date: December 21, 2015

Recipient: Sandia National Laboratories

Address: 1515 Eubank, S. E.
Albuquerque NM, 87123

Website (if available) www.sandia.gov

Award Number: DE-EE00029092

Project Team: Sandia National Laboratories

Principal Investigator: Jason Neely, PMTS
Phone: (505) 845-7677
Email: jneely@sandia.gov

Business Contact: Shannon Boynton
Phone: (505) 284-2303
Email: sboynto@sandia.gov

Technology Manager: Guohui Yuan, Guohui.Yuan@EE.Doe.Gov

Project Officer: Christine Bing

Grant Specialist: -

Contracting Officer: -



U.S. DEPARTMENT OF
ENERGY



**Sandia
National
Laboratories**

Executive Summary:

Increasing the penetration of distributed renewable sources, including photovoltaic (PV) sources, poses technical challenges for grid management. The grid has been optimized over decades to rely upon large centralized power plants with well-established feedback controls, but now non-dispatchable, renewable sources are displacing these controllable generators. This one-year study was funded by the Department of Energy (DOE) SunShot program and is intended to better utilize those variable resources by providing electric utilities with the tools to implement frequency regulation and primary frequency reserves using aggregated renewable resources, known as a *virtual power plant*. The goal is to eventually enable the integration of 100s of Gigawatts into US power systems.

Virtual power plants (VPPs) consist of a centralized controller connected to multiple renewable distributed energy resources (DERs) with advanced grid functionality. By programming autonomous functionality into VPP devices (e.g., PV inverters), the aggregated resources within the VPP act collectively as a dispatchable primary frequency reserve generator. Specifically, this investigation focused on the use of existing IEC 61850-90-7 grid support functions (ie. FW22 frequency-watt function). Since application of the FW22 function requires PV curtailment in this study, this project also investigates the trade-offs between reduced energy delivery and dynamic performance. This approach mitigates the frequency disturbances associated with increased renewable penetration without incorporating expensive energy storage systems or supplemental generation.

Since island grids are promising early adopters of high-penetration PV implementations, this project investigates the optimization of FW22 parameters on an island grid, in particular, the Lanai, Hawaii grid. In depth simulation studies of Lanai are conducted that consider both the day-long aggregate PV behavior as well as the fault behavior of the system. Simulation models included PV power conversion models, based on the wavelet variability model, which computed PV power using irradiance data from Lanai. Since the Lanai power system is already operating at a 20% PV penetration level, these models were validated at 20% penetration using frequency data collected at Lanai along with the irradiance data. Both energy and frequency performance outcomes were compared to help evaluate the tradespace for FW22 parameter selection, and the relationship between FW22 parameters and performance/energy figures of merit (FOMs) was determined using Latin Hypercube Sampling (LHS) based simulation experiments. By relating the frequency performance outcomes and energy outcomes to grid operator costs, a FW22 implementation price was determined for 20%, 70% and 120% penetration scenarios.

The overall project was successful, completing each of the project tasks which included objectives for model development, simulation, FW22 parameter sensitivity analysis and optimization. The project successfully discovered key relationships between FW22 parameters and key FOMs, and even established a technique for finding the most economical FW22 curve for a power system. In particular, the optimization results indicate a daily average savings of greater than \$20k may be realizable with FW implementation on the Lanai power system in high-penetration scenarios. In short, this project demonstrates the value of FW22 function implementation and answers the

question of how best to select FW22 parameters as a function of PV penetration level. Furthermore, the models were developed on commercial software platforms, including MATLAB and Positive Sequence Load Flow (PSLF), which are already widely used for utility R&D. The models and lessons learned with the Lanai island grid simulations will be transferable to studies of larger grids, such as the western North American Power System (wNAPS). These tools will thus be invaluable to utility operations and planning. The outcomes of this project will accelerate the implementation of the FW22 function which in turn will enable accelerated adoption of PV.

Table of Contents

Executive Summary	2
Background	5
Lanai Island Grid	5
Frequency-Watt Function.....	6
Advanced Grid Function Deployment.....	6
Wavelet Variability Model.....	8
Project Objectives	9
Project Results and Discussion	11
Dynamic Model development.....	11
MATLAB Model.....	11
PSLF Model	15
PV Profiles.....	15
Model Validation.....	17
Simulations	18
LHS Results	24
Figures of Merit.....	24
Monetary Cost Model.....	29
Optimization Method.....	31
Hardware Experiments.....	33
Significant Accomplishments and Conclusions.....	37
Inventions, Patents, Publications, and Other Results	38
Path Forward	39
Funding Statement.....	39
References	40

Background:

The simulation and optimization studies presented herein are based on high-fidelity models of the Lanai power grid with frequency-watt function deployment and irradiance variability. This section provides background on the Lanai island grid, the frequency-watt function, advanced grid function deployment in general, and the Sandia-developed wavelet variability model for computing available PV power from irradiance data.

Lanai Island Grid

Hawaiian Electric Co. (HECO) and the Puerto Rico Electric Power Authority (PREPA) have created strict interconnection requirements for PV and wind projects. As a result, PV systems must be co-located with expensive smoothing batteries. The requirements are driven by fears that the variability of renewable generators will no longer allow traditional generators to balance load and generation and there will be large frequency swings. These strict, expensive requirements could be lightened if the entire system was stabilized (as opposed to smoothing each plant individually). One method would be proper application of grid support functions in the power electronics connecting the renewable sources to the grid. A previous study of a 1.2 MW PV plant in Lanai, HI showed that real power curtailment is an effective tool to reduce PV ramp rates and assist with frequency stability [1]. Unfortunately, when performing this control strategy, there is often unused DC power 'left on the array.' In this project, an island grid (e.g., Lanai, HI) will be modeled and assessed in simulation with different PV penetrations and different grid support function controller settings. Lanai is a 140.5 square mile Hawaiian island with approximately 3,200 residents in 1,150 households, living mostly in Lanai city. Figure 1 presents an overview of the power system [1] which includes a 10.4 MW diesel power plant, three 12.47 kV distribution circuits [2], 6 MW peak load and the La Ola PV power plant.

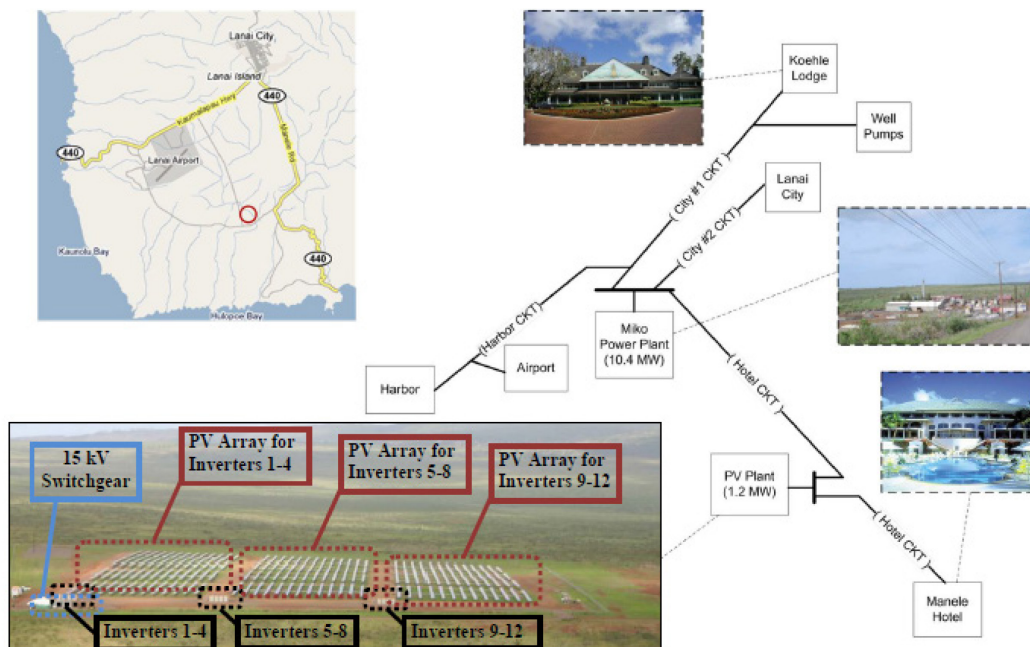


Figure 1: Overview of the Lanai Power System

Frequency-Watt Function

Inverters that implement advanced grid functions have the ability to assist with bulk system frequency problems, distribution-level voltage deviations, and provide additional protection and resiliency to the electric power system. These capabilities come at limited expense but can greatly increase the penetration of photovoltaic and other renewable energy on the grid, reduce the size of ancillary services, and provide wide-area damping control. This project focuses on the frequency-watt function.

The FW curve is either defined through parameters, such as in the German VDE-AR-N 4105 [3], or with a pointwise method, such as in the IEC 61850-90-7 FW22 function [4]. In this report, we define pointwise FW curves. The FW22 settings are given by four pairs of points that define a relationship between power and frequency: (F_1, GP_1) ... (F_4, GP_4) ; these are illustrated in Figure 2. Since the approach relies on curtailment to provide the generator headroom, instead of energy storage or generation, there exists a trade-off between power opportunity cost and frequency response performance; this trade-off will be investigated and quantified for the selected scenarios with different penetrations. Simulating different frequency-watt curves on island grids will demonstrate the benefits of this approach, determine appropriate FW22 settings, and provide the basis for experimental work in the future.

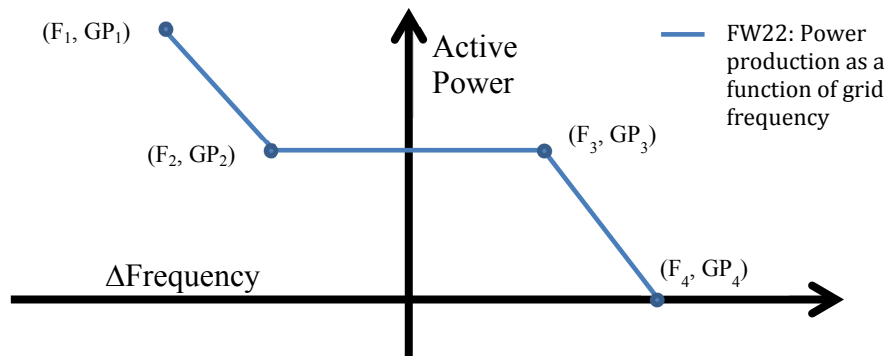


Figure 2: Example frequency-watt curve with a deadband which curtails the output power at nominal grid frequency, increases generation at low grid frequencies, and decreases generation when the grid frequency increases.

Advanced Grid Function Deployment

Many advanced grid functions are required in Europe and, more recently, in certain jurisdictions in the United States. Advanced grid functions (AGFs) in photovoltaic and energy storage inverters have been mandated in national grid codes for low and medium voltage interconnections in Italy, Spain, Germany, Austria, France, and other European nations [5]-[6]. These functions include low and high voltage ride through (L/HVRT), active power as a function of grid frequency, reactive power injection/absorption, and remote disconnection requirements [7].

In the United States, many jurisdictions are considering modifications to the distributed energy resource (DER) interconnection requirements to utilize renewable energy and energy storage systems to support grid frequency and voltage. California

has modified the Electric Rule 21 Tariff to include several AGF implementations in order to help CA utilities meet aggressive renewable energy targets [8]-[9]. In January 2013, the California Public Utilities Commission (CPUC) convened the Smart Inverter Working Group (SIWG) composed of state agencies, utility engineers, national laboratories, manufacturers, trade associations, and advocacy groups to provide consensus AGF recommendations to the CPUC [10]. Pulling from the AGFs defined in the International Electrotechnical Commission (IEC) Technical Report 61850-90-7 [4], the SIWG recommendations were split into three-phases of deployment [10]:

- Phase 1 – autonomous functions, e.g., volt-var and frequency ride-through
- Phase 2 – communication functionality
- Phase 3 – advanced functions requiring communications, e.g., real power curtailment

In December 2014, the CPUC commissioners unanimously ratified the first phase of the SIWG recommendations, and it is expected that CA Rule 21 will require the second two SIWG phases in the near future.

While certification and testing of advanced DER/inverter functionality is a major area of pre-standardization [11]-[13], selection of AGF parameters are also key to the successful deployment of the new technology. Just as the distributed controls of conventional generation must be harmonized to establish robust grid performance, the AGF parameters—e.g. curve shapes (deadbands and slopes), ramp rates, and delays—will become increasingly relevant as renewable penetration increases. In particular, unintended emergent behavior from untuned distributed controls can disrupt the grid as opposed to supporting it.

The potential for disruption has been exemplified by the “50.2 Hz problem” in Europe, wherein a minor high frequency event would trip off gigawatts of distributed generation and lead to bulk system destabilization [14]. This will ultimately lead to expensive retrofits to more than 400,000 inverters [15] to adjust the must-trip L/HFRT settings and add new frequency-watt functionality which gradually reduces output power of DER as the frequency increases above 50.2 Hz [15] according to VDE AR-N 4105 [3]. To further mitigate this issue, PV systems in Germany rated for less than 30 kW must limit their power to 70% of nameplate capacity or disconnect when the Distribution System Operator (DSO) sends the DER a signal; larger systems must have the remote DSO disconnection capability [16]. For this reason, detailed analyses of the desired and unintended grid effects must be performed prior to selection or standardization of AGF parameters.

While European codes strictly define the parameters for AGFs, in California, there are default settings with wide ranges of adjustability for grid-support functions [17]-[18]; thereby allowing utilities to adjust the settings as necessary for their jurisdiction, but transferring the burden onto them to select settings which have not been standardized across the industry. To advise utility regulators in these jurisdictions, high-fidelity, analytical studies and field experiments are necessary to determine proper advanced DER settings.

Many researchers have investigated different advanced grid settings for grid support behaviors. For example, voltage control on distribution circuits (volt/var, fixed power factor, etc.) to increase the hosting capacity and maintain the circuit within the required voltage limits were studied in [19]-[24]. Similarly, Winter *et al.* investigated volt-watt functions for increasing the hosting capacity in Europe [24]. While wind [25]-[26] and energy storage systems [27] are more commonly studied for frequency control, optimal frequency control settings—such as IEC 61850-90-7 frequency-watt functions—have been studied recently to provide wide-area damping [28], and mitigate frequency disturbances and provide primary frequency reserves and/or regulation [29]-[34]. Some of the gaps in this research include the use of the PV system for ancillary services, such as balancing energy loss (from curtailment) to provide frequency response during an $N-1$ contingency event.

This research project aims to optimize the FW22 functions for primary frequency control reserve. This capability is critical for contingency events when generation is lost or when there is a transmission failure. Many $N-1$ studies are often performed by utilities to ensure their system's resilience. The fault tolerance is determined by simulating the loss of the largest generator on the system and determining the frequency drop as the reserves stabilize the grid frequency. In cases where the frequency drops too far, load shedding (e.g., Standard PRC-006-1) and other emergency procedures will engage, eventually leading to a complete blackout. In order to prevent this situation with high penetrations of PV or other renewables, the DER should participate in frequency reserves to serve that role of the traditional generators they've displaced.

This research remains critical to the long-term resiliency of island grids as renewable penetrations continue to increase. HECO is facing increasingly severe fault scenarios due to the displacement of traditional generators. It is believed that the results from this project will aid in scoping grid requirements in HI.

Wavelet Variability Model

PV power output samples were created based on irradiance measured at the 1.2 MW La Ola PV plant on Lanai. Irradiance data was available at 1-second resolution. This point sensor measured irradiance was scaled to plant-average irradiance which accounts for the spatial smoothing across the spatial extent of the PV plant or plants to be simulated. This was done to allow for simulation of any size PV plant – using measured power output from the La Ola plant would only be representative of the 1.2 MW case.

To compute available power, the wavelet variability model (WVM) was used [36] to smooth the irradiance at each simulation location. The WVM decomposes the irradiance signal by timescale using a wavelet transform and then applies different amounts of smoothing at each timescale based on the distance traveled by cloud shadows at that timescale relative to the distance between PV modules. At long timescales, cloud shadows travel long distances, even distant PV modules are highly correlated, and there is little smoothing across the PV plant. Conversely, at short timescales there is little correlation between PV modules and hence significant smoothing. Specifically, the WVM takes the amount of PV, the PV density, and the daily cloud speed (see diagram in Figure 3) as inputs. For this work, the PV density was assumed to be $40 W_{ac}/m^2$ for

utility-scale PV plants (such as La Ola) and $5 W_{ac} / m^2$ for distributed PV (i.e., rooftop). These values are consistent with the ~ 6 acres per MW ($41 W_{ac} / m^2$) found in a survey of utility-scale PV plants [37], and with the $\sim 7.5 W_{ac} / m^2$ found for the very dense rooftop PV (80% of houses have PV) in Ota City, Japan. The daily cloud speed was assumed to be 10 m/s, which is realistic for Hawaii [39]¹.

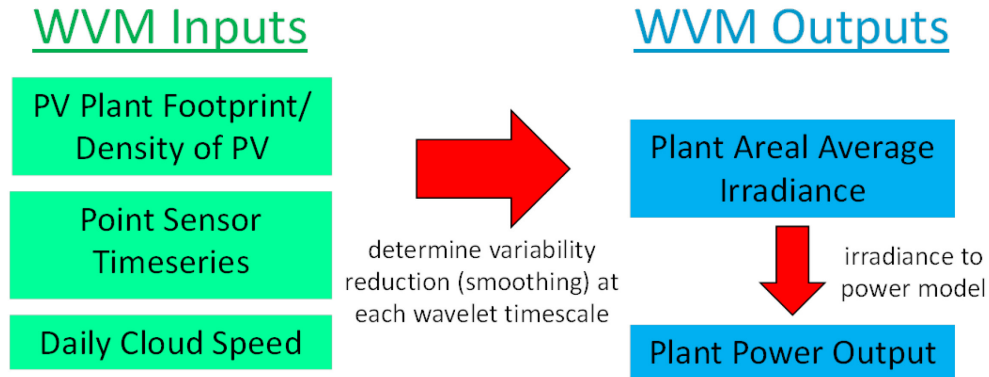


Figure 3: Inputs and output for the wavelet variability model (WVM).

The output of the WVM is plant area average irradiance on the same plane as the irradiance point sensor used as input to the WVM. This average irradiance was converted into AC power output using the Sandia Array Performance Model (SAPM) [41] and the Sandia Inverter Model (SIM) [42]. Since the exact make and model of inverters at La Ola and other (hypothetical) PV plants to be simulated was not known, SunPower SP305 305 W monocrystalline modules were assumed in the SAPM and the SMA America SC 500HE-US 500 kW inverter was assumed in the SIM. While module and inverter technology assumptions are required to run the SAPM and SIM, these assumptions are expected to have little effect on AC power simulations; differences in AC power output for similar modules or inverters are expected to be much smaller than the variability in power output due to irradiance differences. The DC to AC ratio (i.e., the ratio of W_{dc} of PV modules to W_{AC} of inverter capacity) of the fixed tilt modules was set to 1.05, roughly cancelling out the assumed DC derates of 0.94 at solar noon.

The resulting AC power output created using the WVM, SAPM, and SIM will have variability representative of the true variability of the size of PV plant simulated. This procedure has been validated at other PV plants [43]-[44], and is expected to have similar accuracy at the Lanai location.

Project Objectives:

The purpose of this project is to develop tools/analyses that enable electric utilities and other stakeholders to incorporate more photovoltaic (PV) resources without causing adverse frequency response. These tools will provide utilities with the ability to configure specialized functions to achieve frequency regulation using a collection of distributed

¹ For locations in the continental United States, a database of numerical weather forecasted cloud speeds is typically used [40], but this data base does not cover Hawaii.

renewable resources, aggregated into a *virtual power plant* (VPP). The project investigates the use of existing IEC 61850-90-7 grid support functions to accomplish frequency regulation or improve frequency response using a frequency-watt function (specifically the FW22 function) and determines the trade-offs between reduced energy delivery and dynamic performance. This approach allows for mitigation of the frequency disturbances associated with increased renewable penetration without incorporating expensive energy storage systems or supplemental generation.

Custom validated models are developed to aid in understanding the effect of frequency-watt implementation on energy curtailment, on frequency deviation and on fault response. These models are then used for frequency-watt function parameter optimization in an island grid. The project subtasks are as follows:

1. Simulate ramp rates for different PV plant sizes using irradiance data from Lanai in MATLAB for FW22-enabled and FW22-disabled PV plants.
2. Determine energy reduction (loss), ramp rates, and grid frequency for a given set of FW22 parameters in MATLAB.
3. Build PSLF simulations of Lanai's electricity grid with PV inverters with frequency-watt functions. In contrast to the MATLAB model of a PV plant subject to irradiance profiles, the PSLF model will include dynamic components associated with diesel generators, transmission line reactance and loads encompassing the whole island.
4. Optimize the FW22 parameters based on a weighted fitness function; dynamic simulations will be done in MATLAB and PSLF, and fitness function evaluation and post processing will occur in MATLAB
5. Analyze simulation results to identify advantages and disadvantages of the VPP implementation, including a determination of whether there are any unintended emergent behaviors.

It is noted that since control action is being incorporated into the PV systems themselves, this scheme is intended to scale very well with increased PV penetration. The objectives above were selected to help develop tools and demonstrate scalability of the approach on an island grid model; however, it is expected that these tools and properties will be applicable to much larger power systems in the continental US. By addressing the engineering problem of increased frequency fluctuation, this project helps to enable greater adoption of PV across the continental US. In addition, by modeling and minimizing cost, the work addresses the issue of cost effectiveness. Thus, this project addresses several of the objectives that the SunShot Systems Integration program has identified as key to achieving 100s of GW of solar penetration in US power systems.²

² <http://energy.gov/eere/sunshot/systems-integration>

Project Results and Discussion:

In this project, high-fidelity models of the Lanai power grid were developed in MATLAB and PSLF. These models were validated against field data for the 20% penetration case and then augmented in order to generate hypothetical 70% and 120% penetration cases. Herein, penetration level is defined according to Equation (1),

$$\text{Instantaneous PV Penetration (\%)} = 100\% \cdot \frac{\text{Total PV Installed Capacity}}{\text{Peak Load of Power System}} \quad (1)$$

where total PV installed capacity is the sum of the nameplate AC capacities of all PV systems. Total PV installed capacity is typically much less than the power system load, and conventional generation is required to provide most of the power and regulate the frequency of the system. As the PV power penetration increases (relative to load), less conventional generation is dispatched, and variability in the PV power tends to contribute to frequency fluctuations. If available PV power is greater than load, then curtailment is required or, alternatively, energy storage must be engaged to store the excess energy. In this study, the frequency-watt function enacts some curtailment at the nominal frequency but also makes the system responsive to frequency changes, allowing for a great deal more flexibility.

The dynamic models developed herein were used to characterize the effect of frequency-watt parameters on performance and cost. Two methods were used. The first was Latin Hypercube Sampling for design and evaluation of simulation experiments. The second method utilized MATLAB and PSLF together to optimize FW parameters. Finally, select hardware experiments were done to complement the simulation efforts and investigate practical considerations in a physical system.

Dynamic Model development

The MATLAB model was developed for day-long simulations of dynamic performance given PV variability. The PSLF model was utilized for short-duration simulations of dynamic response to faults and loss of generation.

MATLAB Model

The MATLAB model includes the power calculation for the power plant for the purpose of computing power levels, frequency deviation, and ramp rates over a day-long time period. A one-line diagram of Lanai's power system is shown in Figure 1. The MATLAB model approximates the collection of generators as one rotating mass with the generator inertias and damping coefficients aggregated; the resulting rotor dynamics are given by

$$\frac{d\omega}{dt} = \frac{P_{m1} + P_{m2} + P_{PV} - \Delta P_L - D\omega}{J\omega} \quad (1)$$

where ω is the generator speed in radians/second, P_{m1} is mechanical power in megawatts (MW) of generators in droop control mode, P_{m2} is mechanical power in megawatts (MW) of generators providing isochronous control (i.e., integral speed

control), P_{PV} is total power from photovoltaic sources, ΔP_L is the change in load power consumption from nominal, D is the damping coefficient in MW-s/rad, and J is the rotor inertia in $\text{kg} \cdot \text{m}^2$. The model also includes primary speed control which includes droop compensation and a speed governor; Figure 4 illustrates the simplified model. The model output is electrical frequency in Hertz, which is related to generator speed by $f = 2\pi\omega \frac{P}{2}$ where P is the number of generator poles.

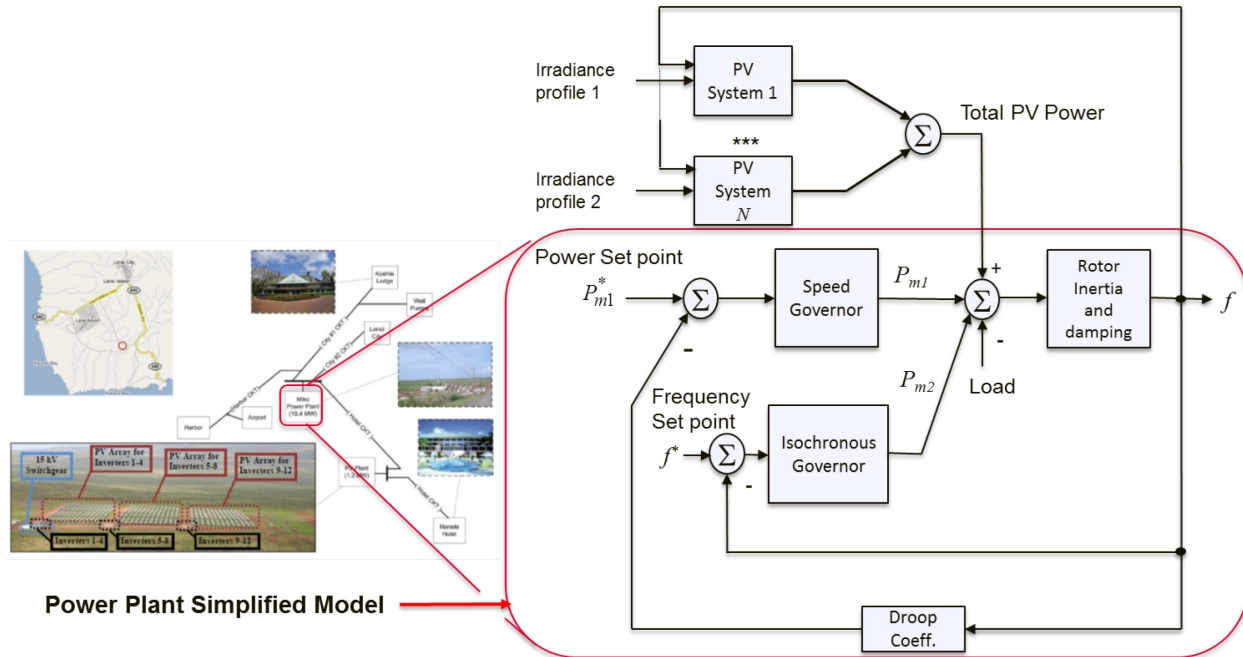


Figure 4: Overview of the simplified Lanai Power System represented in MATLAB

The system dynamics are computed using a four-step Adams-Bashforth integration with fixed time step of 10 msec. Since the available PV power is computed using the WVM with 1-second resolution, intermediate values were determined at the smaller time step using linear interpolation. These intermediate values are adjusted according to the frequency-watt function and applied to the system. Several frequency-Watt function parameter settings were identified for evaluation. The curves are shown in Figure 5 below. Therein, the curves were selected to provide a pair-wise evaluation of the FW function with capacity curtailment. For example, 85% capacity curtailment is best compared with FW22 set 2 since it has the same curtailment at nominal frequency. Specifically, the 85% capacity curtailment and FW22 set 2 act identically within the FW22 deadband, but they differ when frequency deviates outside the deadband. The slopes were selected to be relatively large, and the deadband was selected to be small in the curve definitions. In each case, the frequency points were selected to be $F_1=59.5$ Hz, $F_2=59.98$ Hz, $F_3=60.02$ Hz, and $F_4=60.5$ Hz. Detail on the PV profile selection is provided in a later section.

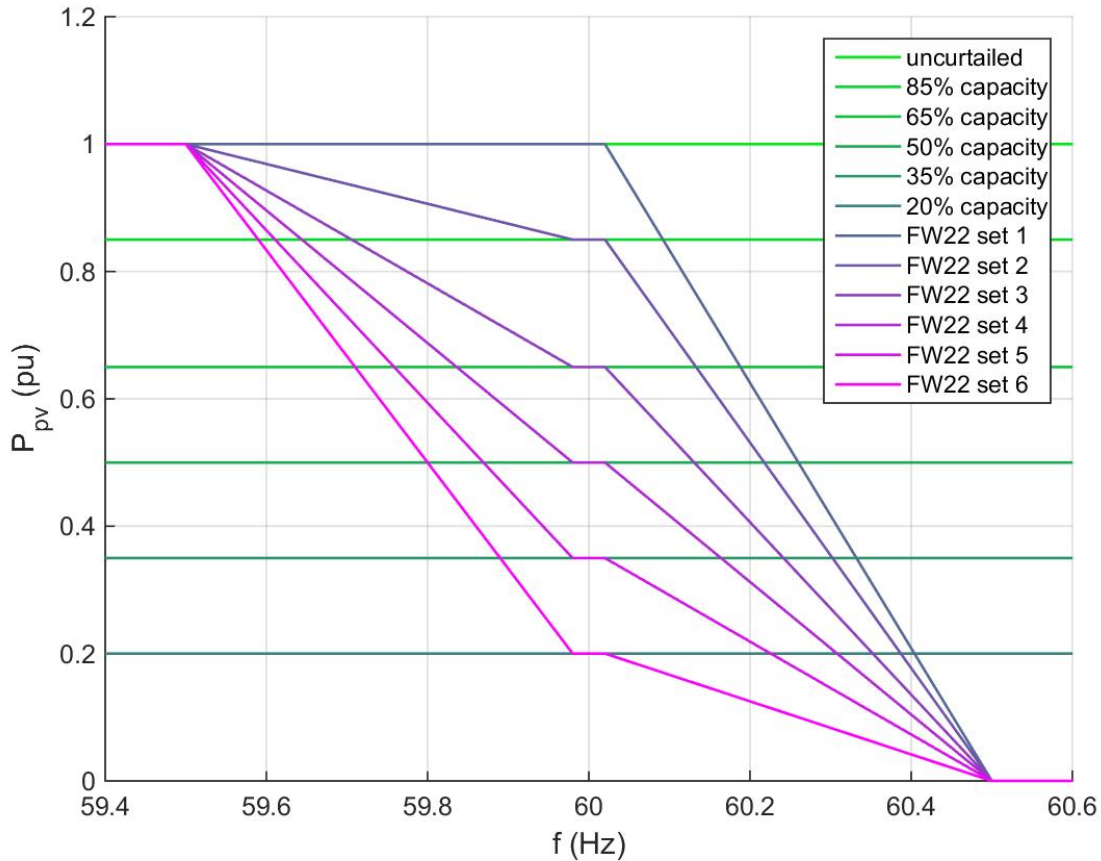
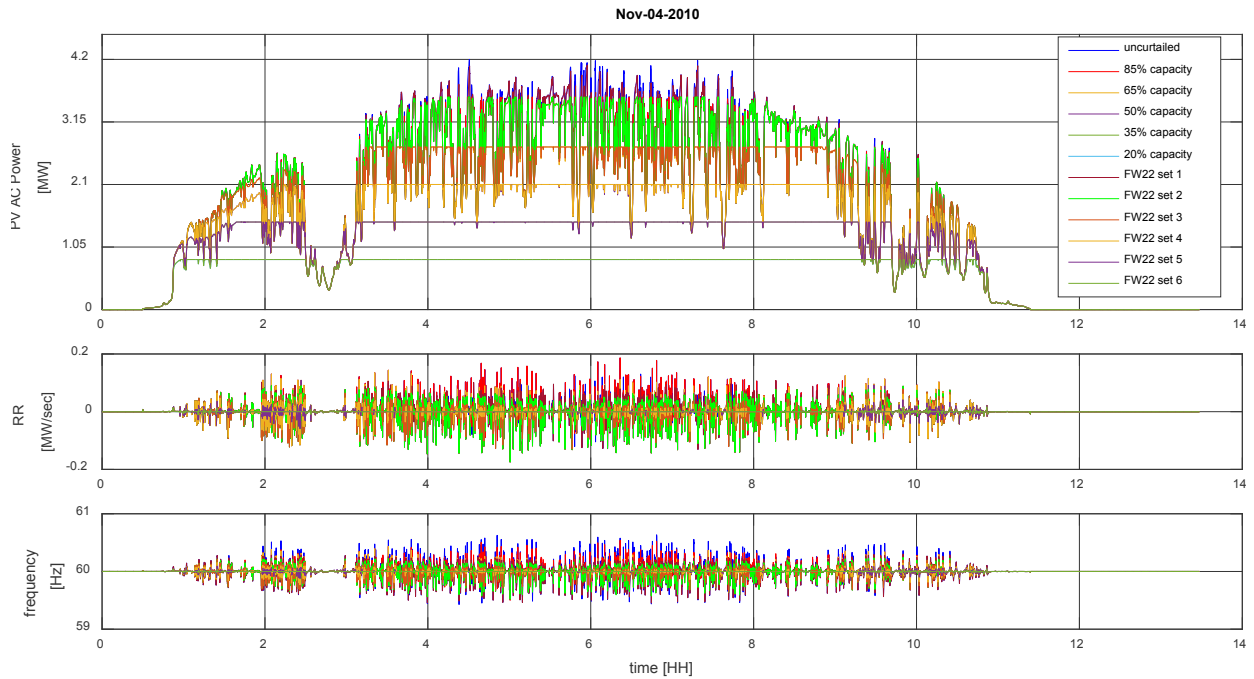


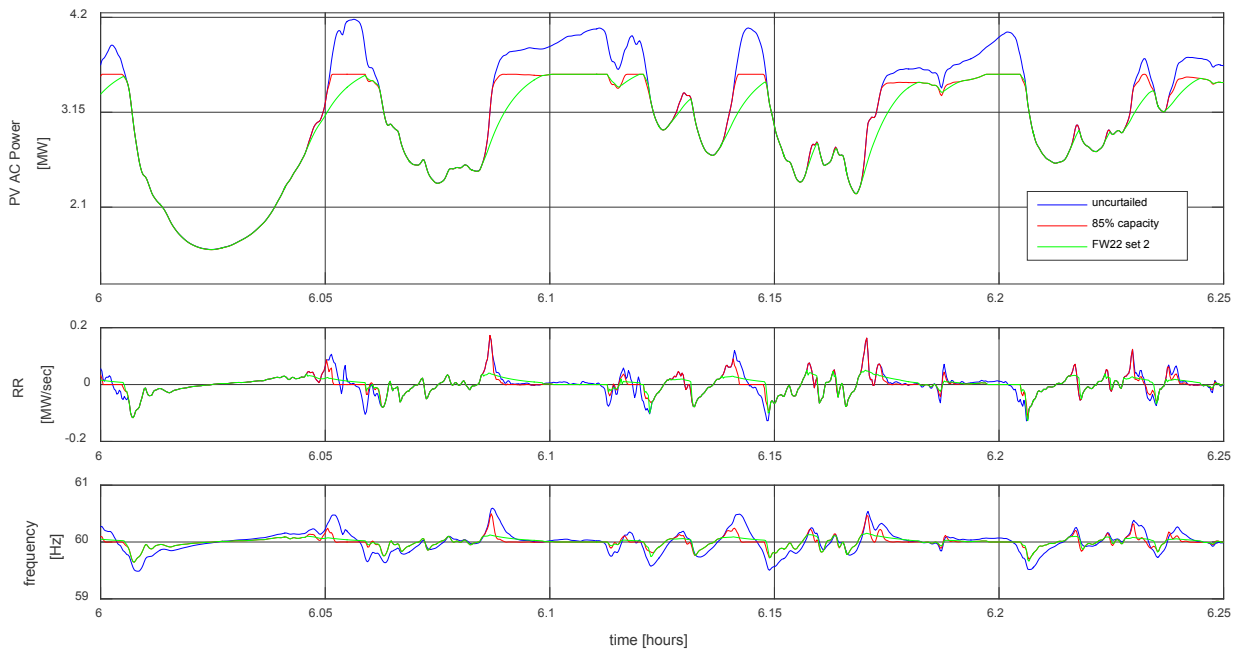
Figure 5: Family of FW22 and capacity curtailment curves, scaled for per unit (pu)

An example simulation output is shown in Figure 6 for different FW parameters and different curtailment strategies. Figure 6a shows the PV power, ramp rates (RR) and system frequency for the November 4th 2010 irradiance profile and all twelve FW cases defined in Figure 5. To illustrate how the PV power is modulated to accommodate frequency, Figure 6b provides a “zoomed-in” view of a high-variability condition for three cases: uncurtailed, 85% capacity curtailment and FW22 set 2. The results are intuitive, and differences in dynamic response are easiest to see for the instances of rapid increase in PV availability. Consider first the uncurtailed case: as available PV power falls, system frequency decreases temporarily until the generator controls compensate by providing additional mechanical power. When the available PV power increases again, system frequency now increases given both the additional mechanical power and the added PV power. This results in a larger overshoot in frequency. The 85% capacity curtailment case, however, caps the PV power at 3.57 MW, which mitigates the PV ramp rates slightly and thus also reduces the overshoot in frequency. In the FW22 set 2 case, however, the PV system responds directly to system frequency and “softens” the rise in PV power. The resulting PV ramp rates and the frequency deviations are mitigated much more than in the curtailment case. It is noted that, in this example, the frequency is never below 59.98 Hz when the available PV power is above 3.57 MW;

thus, the PV power does not rise above this level in this example. An example of PV power rising above the curtailment level is given in the Simulation results.



(a)



(b)

Figure 6: Shows (a) Overview of the simplified Lanai Power System represented in MATLAB with all 12 cases considered and (b) Zoomed-in sample of simulation results for three cases: uncurtailed, 85% capacity curtailment and FW22 set2, from the same MATLAB model

PSLF Model

GE's PSLF software was used to model two grid event scenarios (a generator outage and a line-to-ground fault on a distribution line feeding a well pump) with three PV penetration levels (20%, 70% and 120%) using irradiance data from three different times of day (early morning, late morning and midday). To account for the time-varying PV power availability, pre-calculated Wavelet Variability Model (WVM) [44] PV power values were fed into the 240-second PSLF simulations. The PSLF models were validated against data collected at the Lanai La Ola PV site for the 20% penetration case.

For the higher penetration scenarios, additional PV generators were simulated at the Manele Hotel in Lanai City and the Harbor with time-shifted irradiance profiles that represented a northerly wind direction. Within this model, there were three PV systems (each PV system aggregates multiple inverters) totaling 1.2 MW installed and four diesel generators connected in the 20% case, eight PV systems totaling 4.2 MW and three diesel generators in the 70% case, and thirteen PV systems totaling 7.2 MW with two diesel generators in the 120% case. It is noted that two generators are still necessary in high penetration cases so that *N-1* contingency is satisfied.

PV Profiles

Irradiance profiles were selected to include low variability, moderate variability, and high variability. Variability was quantified using the 99th percentile 1-second ramp: the days with the highest, lowest, and average 99th percentile ramps were selected for study. Additionally, the day with the largest single ramp was included in our analysis. Specifically, the four days (datasets collected at the La Ola Power plant) used for the MATLAB study were:

- December 7th, 2010 – Least Variable (little cloud cover)
- September 3rd, 2010 – Average Variability
- April 23rd, 2011 – Largest Single Ramps
- November 4th, 2010 – Most Variable Total Day

These irradiance profiles are shown in Figure 7.

The PV power calculated depended on whether the PV resource was centralized (PV plant with trackers) or distributed (rooftop solar – fixed plane). Figure 8 contrasts the Dec 7th profile at the La Ola PV plant (central) and in Lanai city (distributed). For the high penetration cases, Lanai city was treated as a distributed resource while Manele hotel and the Harbor were modeled as having adjoining PV plants.

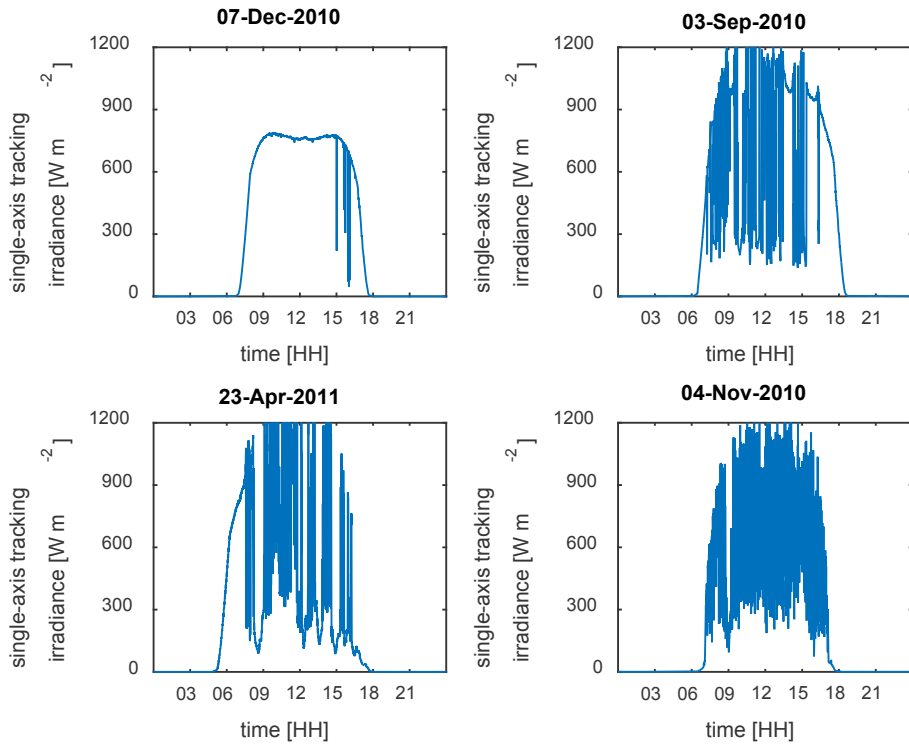


Figure 7: Irradiance Profiles selected for this study were collected from the La Ola PV power plant showing (top left) little variability on December 7th, 2010; (top right) 'average' variability as seen on September 3rd, 2010; (bottom left) April 23, 2011, the day with the largest single ramps; and (bottom right) the day with the highest total variability, November 4th, 2010

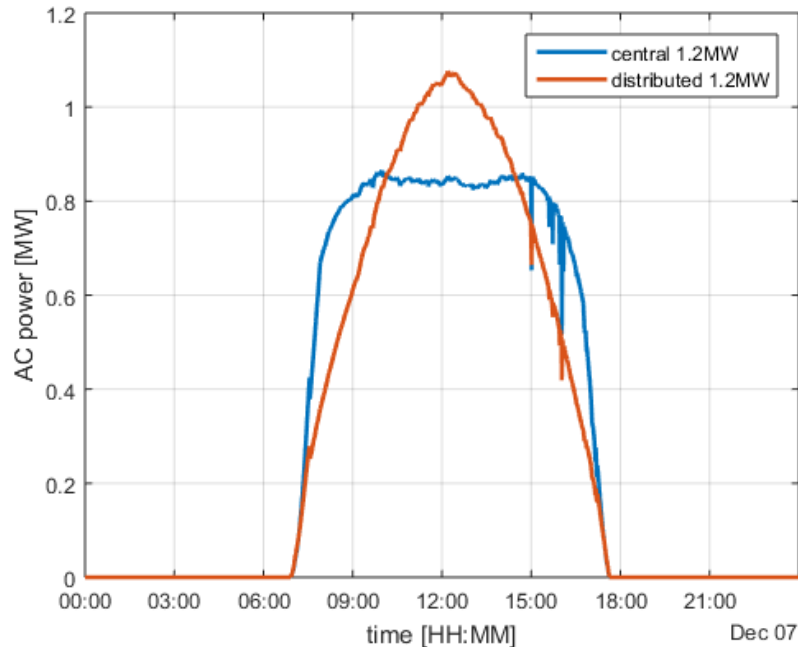


Figure 8: Contrasts the PV power created by centralized PV at the La Ola power plant and rooftop (fixed plane) resources in Lanai City

For each 240 sec PSLF simulations, three different times of day were considered. A family of available PV power profiles were imported to PSLF at the beginning of each simulation shown in Figure 9 for the 120% penetration case.

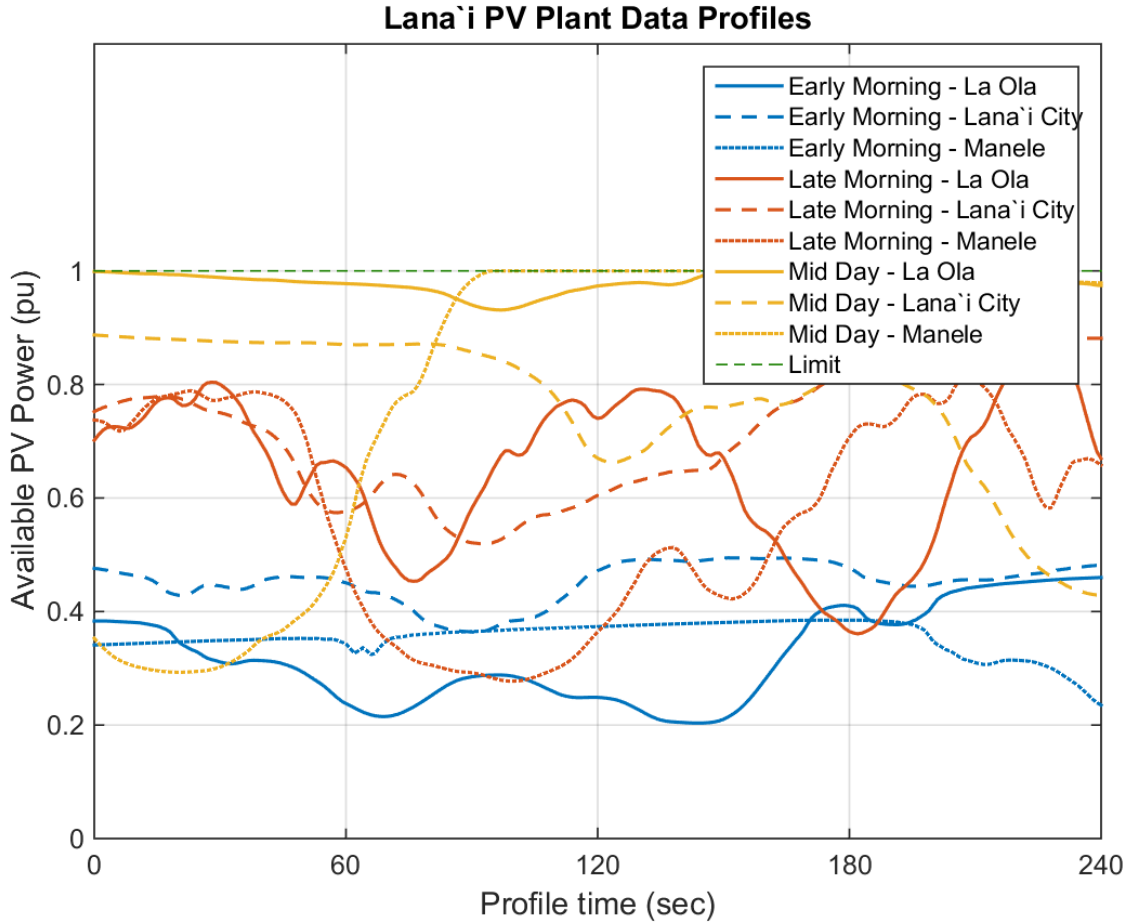


Figure 9: Available PV power profiles computed for PSLF simulation for 120% penetration case

Model Validation

PV power and frequency data were collected at the Lana'i PV power site and stored on an OSIssoft PI server. This server collected data at one second intervals and applied exception and compression rules to reduce the saved data set. These rules are designed to minimize the data set size while accurately representing the data trend. The data used here was reconstructed from compressed data so data points may be spaced more than 1 second apart, but the underlying structure of the frequency response is captured.

The PV profiles were applied in simulation for both the MATLAB and PSLF models for the 20% penetration case. The simulated frequency response was then compared to the measured frequency response at Lanai as seen in Figure 10. Naturally, the physical system was also subject to load variations during this interval; however, load variations were not modeled in the simulations. Nonetheless, good agreement is seen between

the measured and simulated responses since PV variability is the dominant cause of frequency variation in this example. This result is evidence that the MATLAB and PSLF models are representative of the physical system.

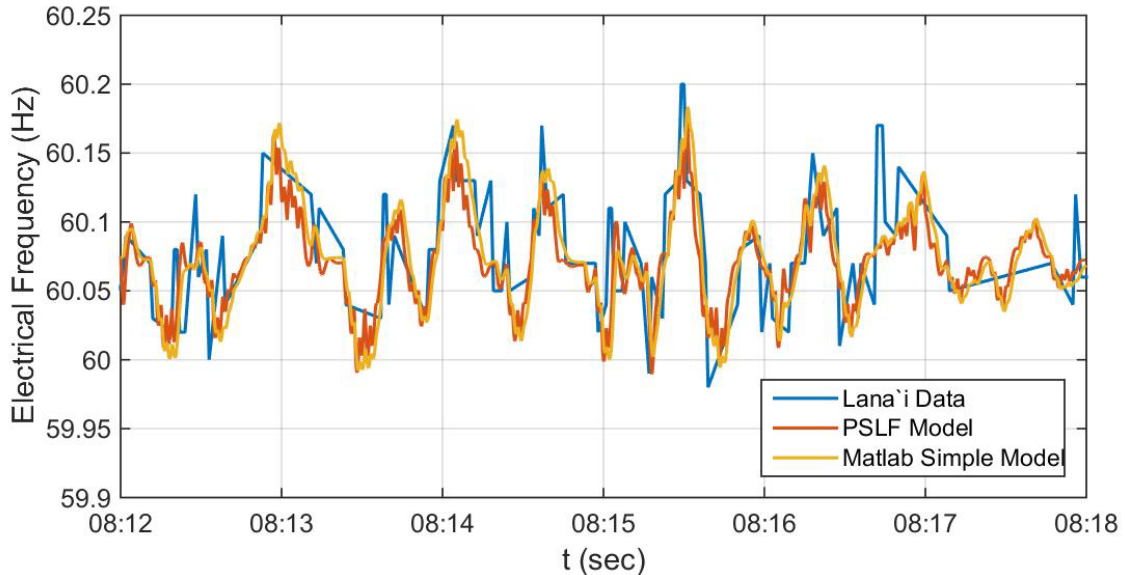


Figure 10: Power and Frequency Comparison between Simulated and Measured Responses using data collected November 4, 2010 (8:12-8:18am shown here) from the Lana'i PV plant

Simulations

The effect of FW function parameters was evaluated in simulation using both the MATLAB and PSLF models. Initial evaluations in Matlab were done to investigate the relationship and trade-off between FW22 parameter selection, ramp-rate and energy loss. Given the different penetration levels, irradiance profiles, and FW22 parameters, several scenario permutations were considered for this study. Specifically, with four irradiance profiles, three penetration levels and six pair-wise comparisons between capacity curtailment and FW22 implementation, 144 simulations were needed. See Table 1 for a summary of scenarios. For the Latin Hypercube Sampling (LHS) and optimization studies, both MATLAB and PSLF models were used. For the MATLAB component of these studies, each FW22 parameter was simulated for a full day using three irradiance profiles and three penetration levels, resulting in 9 simulations. For the PSLF component of these studies, each FW22 parameter selection was simulated for 240 seconds around an event using three penetration levels at three times of day (3 PV profiles), with two events resulting in 18 PSLF simulations. Tables 2 and 3 below summarize these scenarios.

Examples of the MATLAB and PSLF simulations are presented next; the MATLAB simulation example is presented first. To illustrate performance of the PV system under high solar variability conditions, the irradiance data from 11/4/2010 was used, 70% PV penetration (4.2 MW) was used, and the system response was simulated using the FW curves defined in Figure 5.

Table 1: Summary of 144 Matlab Simulation Scenarios for Trade-off Study

Penetration/Profile	December 7 th , 2010 Least Variability	September 3 rd , 2010 Average Variability	April 23 rd , 2011 Largest Single Ramps	November 4 th , 2010 Highest Variability
20% Pen (1.2 MW)	6 FW22 Curves 6 Curtailment levels	6 FW22 Curves 6 Curtailment levels	6 FW22 Curves 6 Curtailment levels	6 FW22 Curves 6 Curtailment levels
70% Pen (4.2 MW)	6 FW22 Curves 6 Curtailment levels	6 FW22 Curves 6 Curtailment levels	6 FW22 Curves 6 Curtailment levels	6 FW22 Curves 6 Curtailment levels
120% Pen (7.2 MW)	6 FW22 Curves 6 Curtailment levels	6 FW22 Curves 6 Curtailment levels	6 FW22 Curves 6 Curtailment levels	6 FW22 Curves 6 Curtailment levels

Table 2: Summary of 9 Matlab Simulation Scenarios for LHS and Optimization Studies

Penetration/Profile	December 7 th , 2010 Least Variability	September 3 rd , 2010 Average Variability	November 4 th , 2010 Highest Variability
20% Pen (1.2 MW)	Select FW22 Curve	Select FW22 Curve	Select FW22 Curve
70% Pen (4.2 MW)	Select FW22 Curve	Select FW22 Curve	Select FW22 Curve
120% Pen (7.2 MW)	Select FW22 Curve	Select FW22 Curve	Select FW22 Curve

Table 3: Summary of 18 PSLF Simulation Scenarios for LHS and Optimization Studies

Penetration/Profile	Early Morning PV Profile		Late Morning PV Profile		Midday PV Profile	
20% Pen	Generator Failure	Line Fault	Generator Failure	Line Fault	Generator Failure	Line Fault
70% Pen	Generator Failure	Line Fault	Generator Failure	Line Fault	Generator Failure	Line Fault
120% Pen	Generator Failure	Line Fault	Generator Failure	Line Fault	Generator Failure	Line Fault

Figure 6 shows the output power, ramp rates, and frequency plotted over time for November 4th. Several performance metrics were obtained and are shown in Figure 11. The ramp rates were defined using the difference between samples of the output power, spaced 1-second apart. The frequency performance was determined by the difference between the maximum and minimum frequency experienced during the simulation of a day. The comparison is best done by comparing markers of the same color; for example, the red filled marker shows the result for the 85% capacity case while the red open marker shows the result for FW22 set 2, which is curtailed the same amount within the deadband. It is noted in Figure 11 that a 85% capacity case results in the 99% ramp rate dropping from 79.6 kW/sec to 78.6 kW/sec and the frequency range drops from 1208 mHz to just 1039 mHz: almost negligible benefit. However, with FW22 set 2, the 99% ramp rates drop to 50.0 kW/sec and frequency range is 739 mHz for a 2% loss of PV energy. The September 3rd, 2010 dataset is evaluated in Fig. 12 assuming 120% penetration (7.2 MW installed PV). In this case, a minimum curtailment is necessary since the installed capacity is greater than load. Therein, large benefits are demonstrated for the use of the FW function. For 35% curtailment, the system frequency deviates 1976 mHz and results in 13% energy loss, but the FW set 3 limits the frequency range to 1271 mHz with 14.2% energy loss.

The energy lost is defined as the percent difference between the PV energy output from a given curtailment scenario and the PV energy available with no curtailment. The ramp rates were defined using the difference between samples of the output power,

spaced 1-second apart. The frequency performance was determined by the difference between maximum and minimum frequencies experienced during a simulated day.

It is noted in Figure 12b that a 15% capacity curtailment results in the 99% ramp rate dropping from 80 kW/sec to 79 kW/sec and the frequency deviation drops from 1200 mHz to just 1025 mHz, almost negligible benefits. However, with FW22 set 2, the 99% ramp rate drops to 50 kW/sec and frequency deviation is 750 mHz for little loss of PV energy. Similarly for each case, the FW22 set results in better ramp rates and frequency deviation performance when compared to its capacity curtailment counterpart. In addition, the energy loss accrued to attain better performance for each is computed.

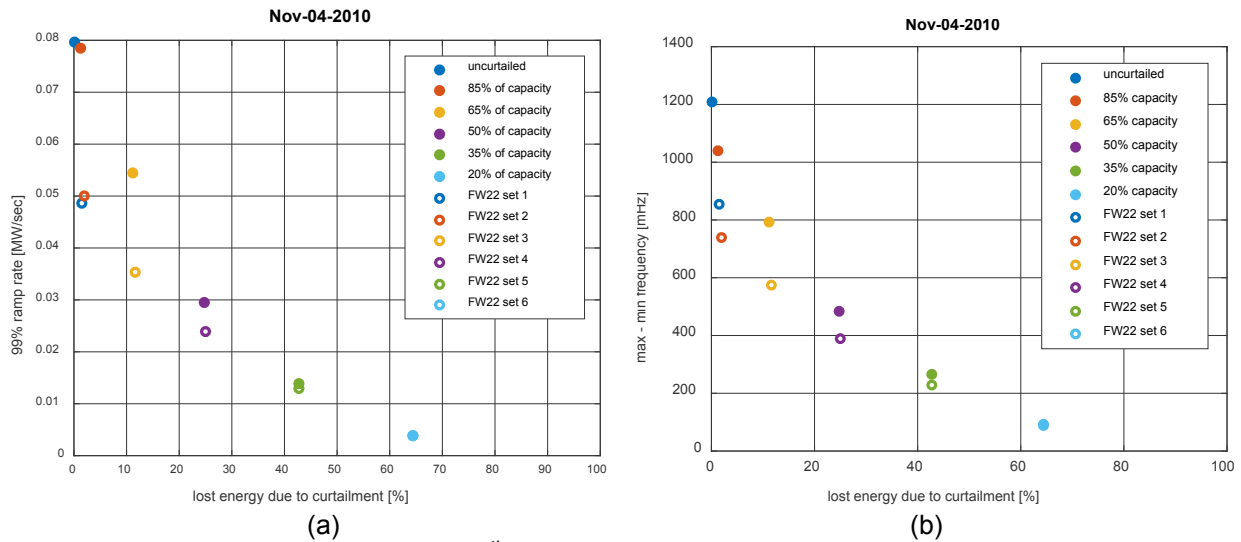


Figure 11: Results for November 4th including plot of (a) ramp rates vs energy loss and (b) frequency deviation vs energy loss.

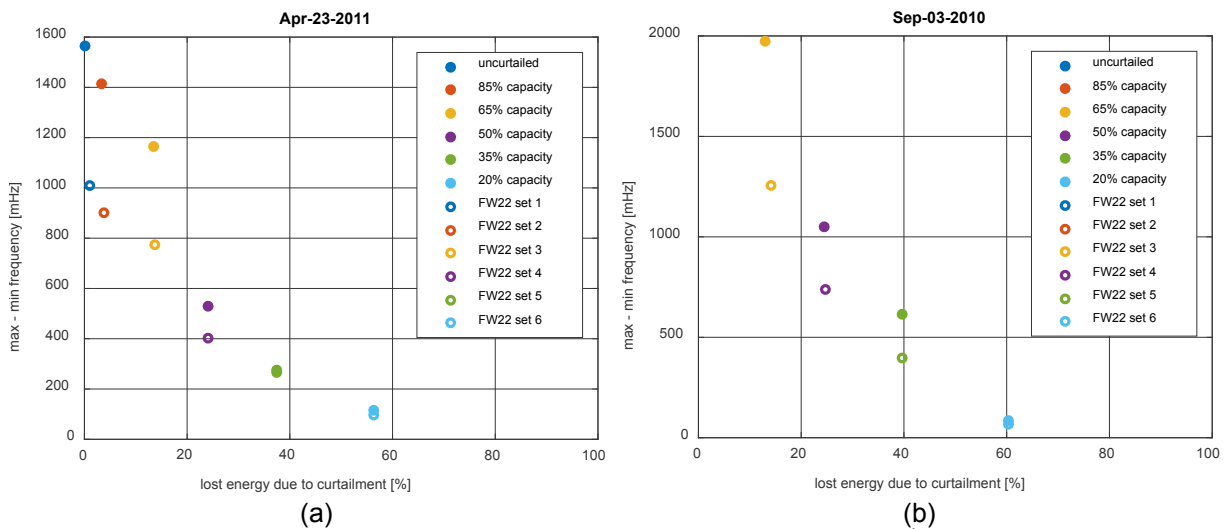


Figure 12: Frequency deviation vs energy loss results for (a) April 23rd, 2011 (b) September 3, 2010.

To further illustrate the potential benefits of the FW implementation in PSLF, two examples are shown below comparing FW implementation to simple curtailment. Both scenarios consider a 70% PV penetration scenario with late morning irradiance profile. The FW curve was defined with $GP_2 = GP_3 = 0.6$, 0.1 Hz deadband, and droop = 1.25 Hz/100%nameplate; the curtailment was defined at 0.6 p.u. for all frequencies; see Figure 13.

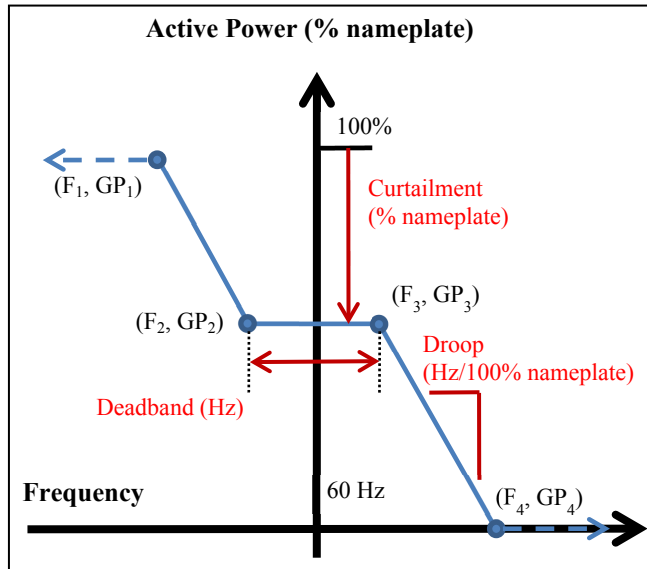


Figure 13: Pointwise FW curve defined using curtailment, droop and deadband

In the PSLF models, four diesel generators were used: Lanai 4, Lanai 5, Lanai 7 and Lanai 8. Lanai 4 and 5 generators were rated for 1.2 MW and regulated using droop control. Lanai 7 and 8 provided isochronous frequency regulation with Lanai 7 acting as primary. All four generators were used for the 20% penetration case, three were used for the 70% penetration case, and two were used in the 120% penetration case. Fig. 14a shows the simulated electrical generator speed for *Lanai 7* generator in the 70% penetration case following loss of *Lanai 5* generator at $t=120$ sec, and Fig. 14b shows the total PV power. The FW and curtailment scenarios exhibit similar response to PV variation since they have the same limit at nominal frequency. However, following the loss of the *Lanai 5* generator, a sizable improvement is seen in frequency response with the FW implementation. The frequency nadir is 59.32 Hz with simple curtailment, but the nadir is just 59.52 Hz with the FW implementation. In addition, the generator speed rises to 60.11 Hz due to PV variation in the curtailment case, but it is limited to 60.05 Hz in the FW implementation. These results are due to the FW control action. In particular, PV power rises by almost 223 kW (to full available power) in the FW case to compensate for the decrease in frequency following loss of generation; see Fig. 14b. The control action is best depicted, however, in the *power-frequency* phase plane together with the FW and curtailment limits; see Figure 15. As the frequency falls below the deadband of the FW curve, the FW limit increases and PV power rises, helping the system to return to nominal frequency. It is further noted that the inverter has its own

dynamics, and the power output may temporarily rise above the FW curve limit during a transient.

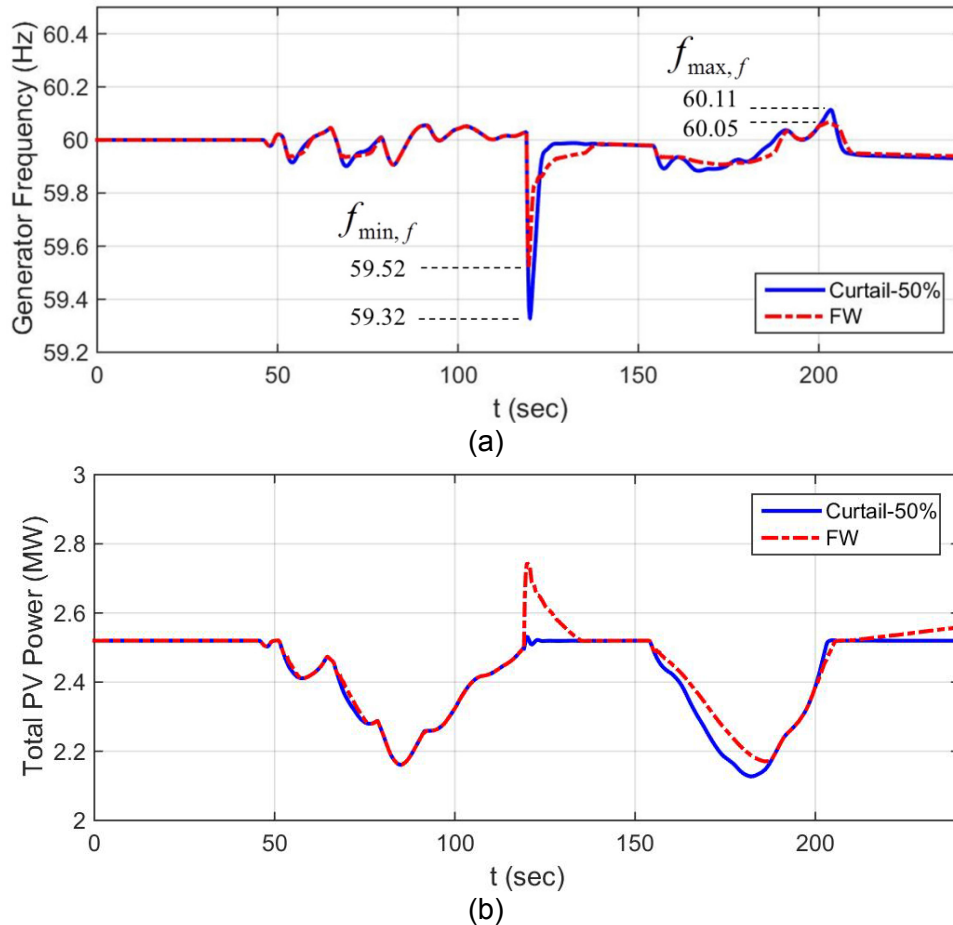


Figure 14: Impact of FW and curtailment for simulated loss of Lanai 5 at $t=120$ sec showing (a) electrical speed of ‘Lanai 7’ generator and (b) total PV power

Figure 16 shows results for a simulated line fault of a medium voltage line feeding a well pump. The fault was modeled as a bolted three-phase to ground fault on a 12.47 kV line located in the vicinity of the component labeled “Well Pumps” connected to the “City #1 Ckt” in the schematic of Figure 1. In simulation, the line is shorted for 100 msec at half its length and then opened. The line-fault causes the generators to speed up until the fault is cleared. As with the previous example, the control action of the FW function mitigates the frequency, resulting in a max frequency of 60.72 Hz compared to 60.55 Hz for the curtailment case. The resultant dynamic response results in a slightly lower minimum frequency however, of 59.76 Hz compared to 59.83 Hz for the curtailment case. As with the loss of generation case, the control action is depicted in the *power-frequency* phase plane together with the FW and curtailment limits; see Figure 17.

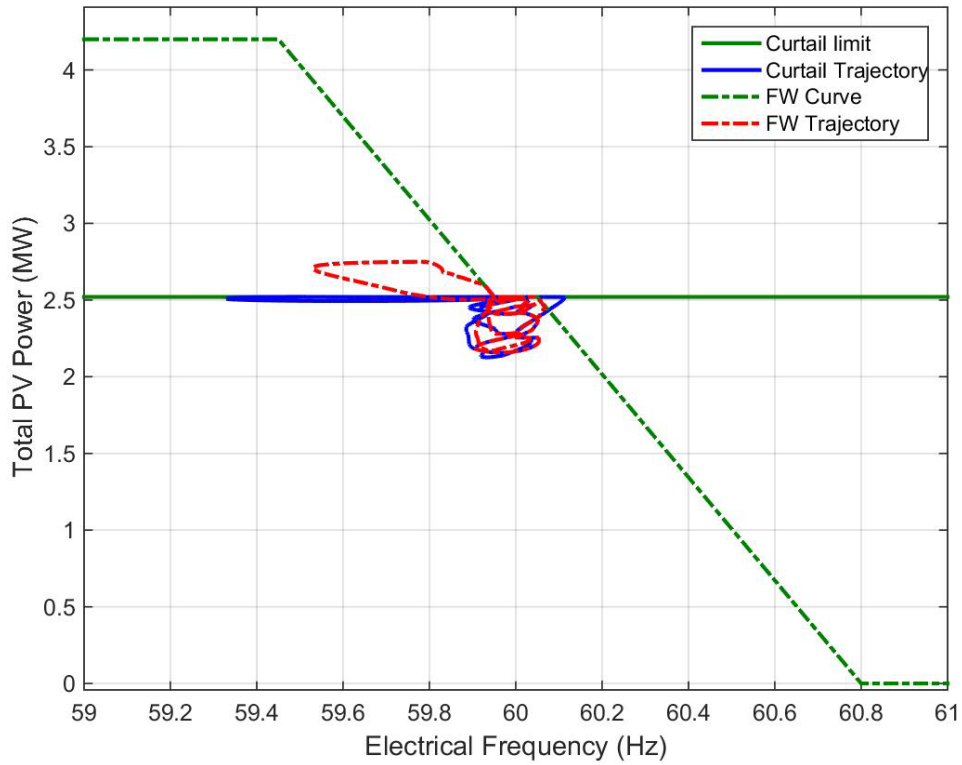


Figure. 15: FW implementation versus simple curtailment, showing response in the PV power as generator speed varies

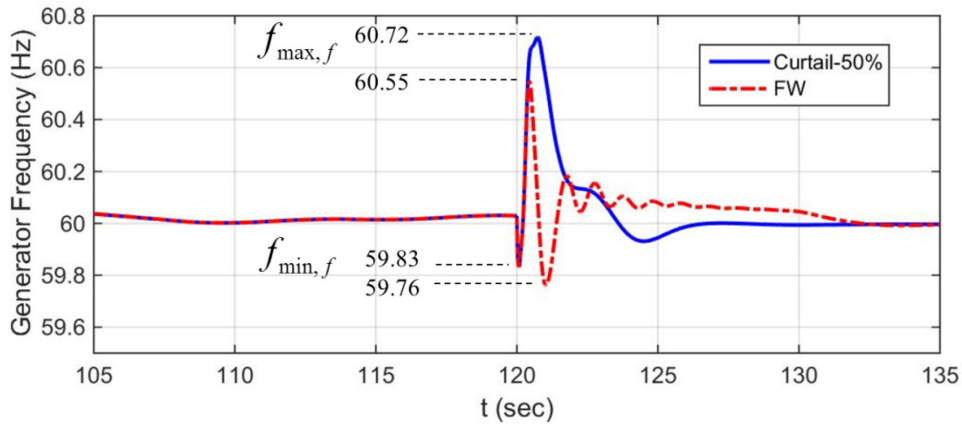


Figure 16: Impact of FW and curtailment for simulated line fault at $t=120$ sec showing close-up of (a) electrical speed of *Lanai 7* generator and (b) total PV power

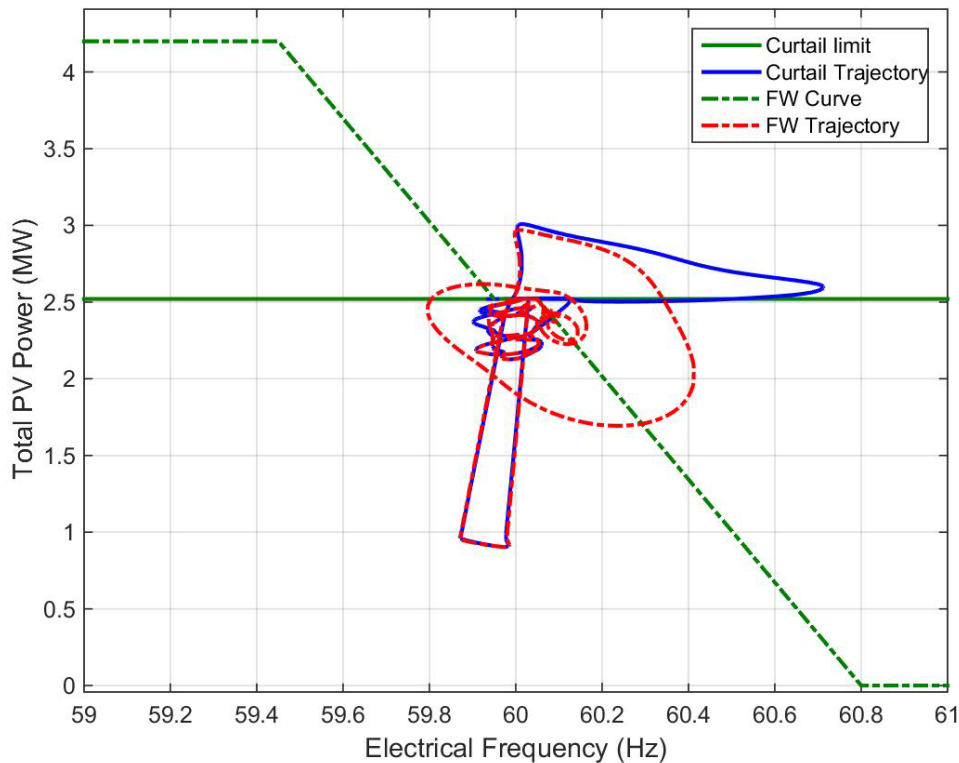


Figure 17: FW implementation versus simple curtailment, showing response in the PV power as generator speed varies

LHS Results

Latin Hypercube Sampling (LHS) enables the intelligent design of simulation experiments and was used to compare the influence of the three FW curve parameters on a number of different metrics (i.e., figures of merit) from the simplified MATLAB power model and PSLF simulations. Unlike a Monte Carlo method (random sampling), LHS ensures the combinations of parameters better cover the design space by subsampling each design variable [45].

Figures of Merit

The FOMs were selected based on the performance of the system for non-event operation subject to variable PV generation and during fault scenarios:

- The maximum (f_{max_f}) and minimum (f_{min_f}) grid frequency measured at isochronous generator *Lanai 7* for the six different PSLF scenarios (two fault types and three times during the day).
- The average energy loss, E_{loss} , for the three days with different irradiance values.
- The absolute minimum (f_{min}), absolute maximum (f_{max}), and average standard deviation (σ) of the Lanai grid frequency for the three simulation days.

The LHS results are shown in Figure 18 for 30 FW curves (in Figure 19) for the three penetration cases. The FW curves were the same for each of the three penetration levels so direct comparisons can be made across the different penetration levels.

The Pearson correlation coefficient, ρ , is displayed for each of the FW parameters with respect to each FOM to help determine the influence of the FW parameter on the metric. The FOM_0 value is the result without the FW function. A first order linear regression is also shown to illustrate the relationship between the FW parameters and the FOMs.

The following general observations can be made from the LHS analysis:

- Curtailment has the strongest influence on the FOMs; in particular, E_{loss} is highly dependent on the magnitude of the curtailment ($\rho_{20\%}=0.973$, $\rho_{70\%} = 0.971$, $\rho_{120\%} = 0.971$).
- As curtailment increases, the frequency range for the non-event and fault cases decreases. This is expected in the 24-hour simulations since the load is fixed and the PV causes the energy imbalance. In the PSLF simulations, the largest curtailment provides the greatest headroom for the PV to respond to the loss of generation event.
- Deadband and droop have less effect on the FOMs.
- An increasing deadband tends to widen the frequency deviation during non-event and fault cases.
- While a minor influence, for the majority of cases, steeper slope (smaller droop) led to more aggressive compensation and decreased frequency deviation. The ability of the FW function to reduce frequency fluctuations increases with greater PV penetration, as evidenced by the larger FOM ranges.

In order to compare the sensitivity of the results to the number of LHS samples, a larger data set was created with 100 LHS samples for the three different penetration levels. See Figure 20. The Pearson correlation coefficient for the results closely matches the 30 sample results indicating that large LHS designs are not necessary to visualize the trends of different FW curve parameters on the FOMs.

As noted in the next section on optimization, when cost modeling is applied and the parameters are optimized to minimize cost, a daily average savings of greater than \$20k may be realizable with FW implementation on the Lanai power system.

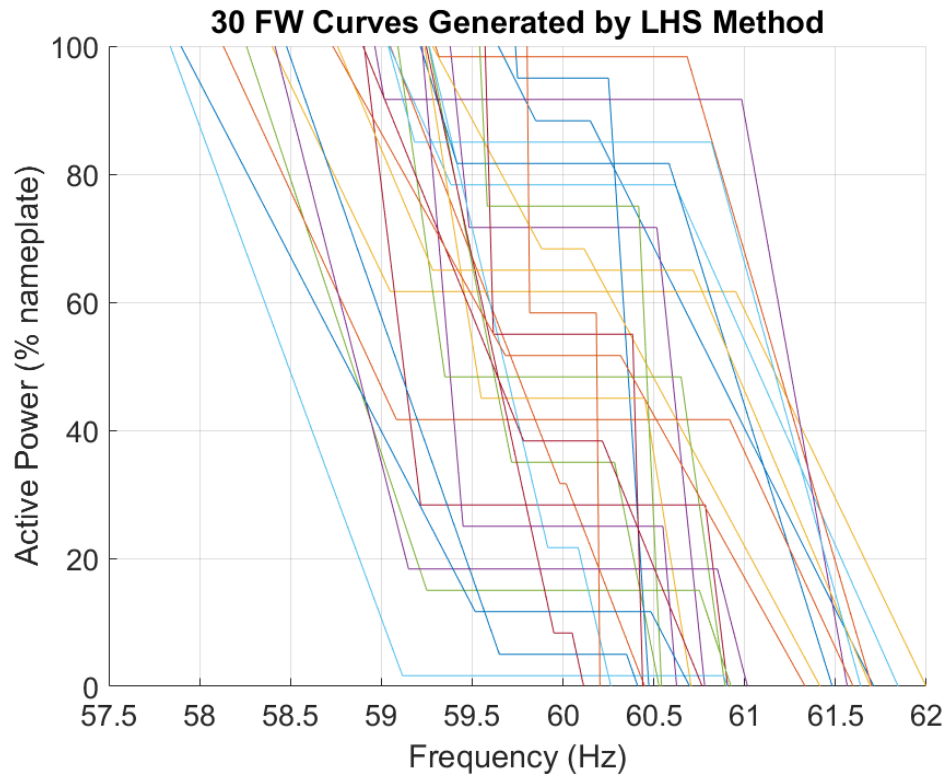


Figure 18: The 30 FW curves used in the LHS analysis.

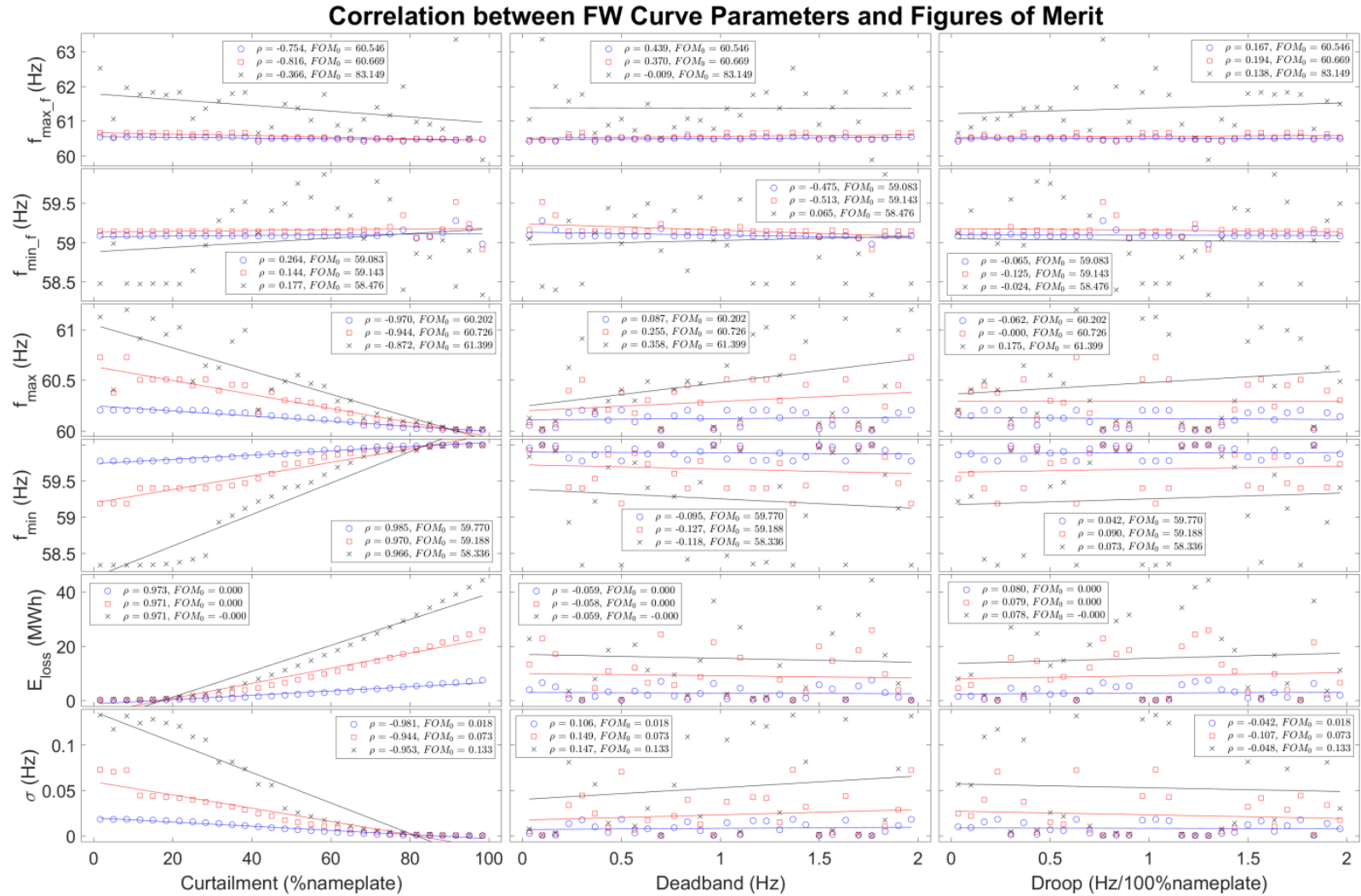


Figure 19: LHS results (with 30 simulations) illustrating the sensitivity of six figures of merit (y-axes) to FW parameters (x-axes) for 20% (blue), 70% (red) and 120% (black) penetration.

Correlation between FW Curve Parameters and Figures of Merit

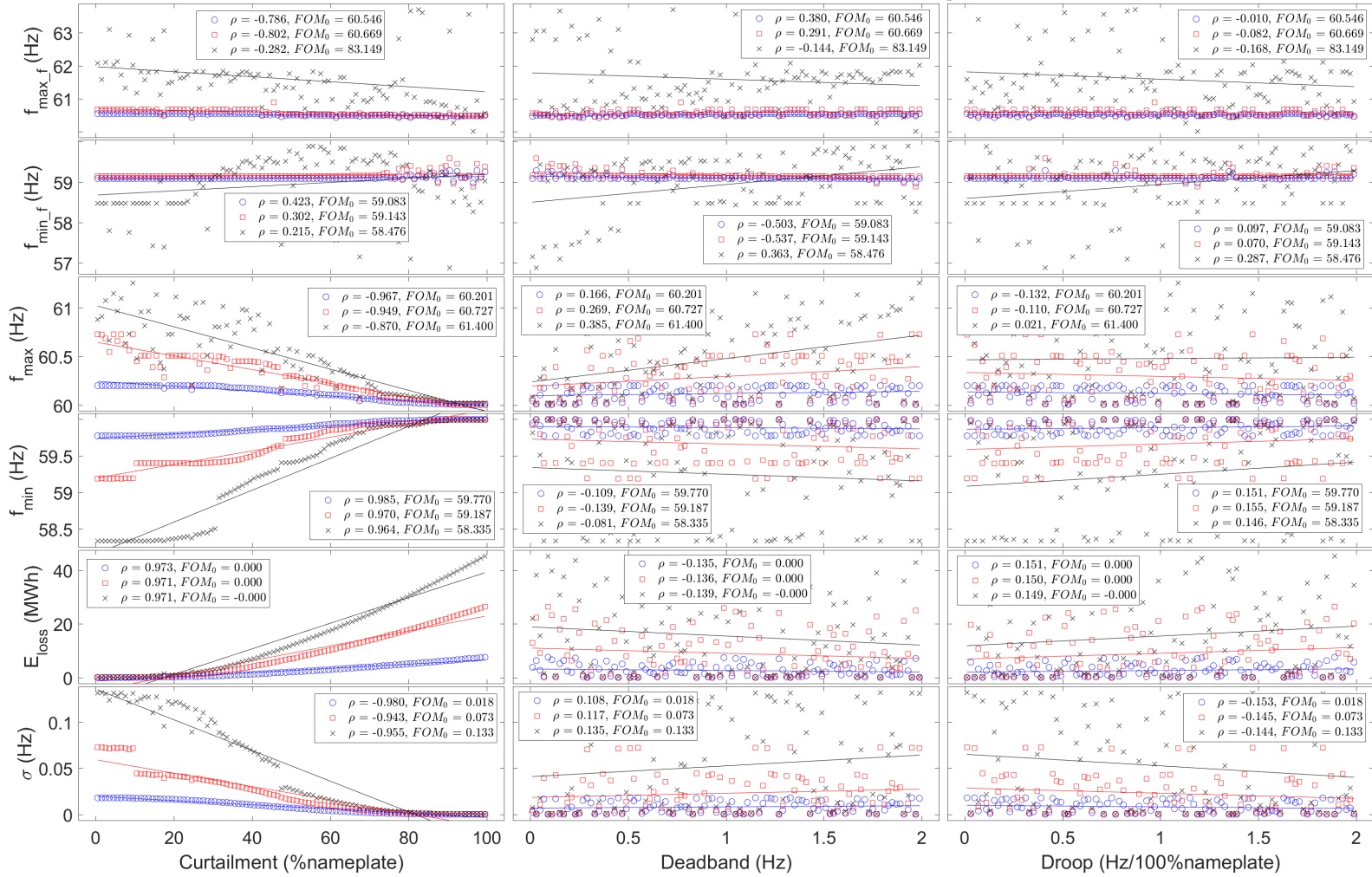


Figure 20: Larger LHS data set (with 100 simulations) illustrating the sensitivity of six figures of merit (y-axes) to FW parameters (x-axes) for 20% (blue), 70% (red) and 120% (black) penetration.

Monetary Cost Model

Utility companies and grid operators would like to implement optimal FW curves for each penetration scenario based on the implementation costs. Different cost functions can be created which produce different optimal FW curves depending on the tradeoff preferences of the utility or system operator. We do not consider the financial implications of increasing PV penetration levels from direct costs or externalities (public health and environmental impacts), but rather, compared costs associated with and without the FW function. By employing renewable energy resources as frequency regulation and primary contingency reserves, the lost revenue from PV production is offset by the reduced service interruption costs and reduced lifecycle costs attributed to generator wear; therefore, three costs were selected:

- The price of the lost energy due to curtailment, calculated from E_{loss} , the average energy lost from the FW curtailment for three days.
- The cost of blackouts, the consumer interruption costs based on f_{min_f} .
- The operations and maintenance (O&M) costs for the synchronous generators associated with grid frequency fluctuations, Δf .

Taking a holistic view of the grid operations, the PV owners should be compensated by the utility for their participation in the contingency response, so the lost revenue from lost energy income due to FW curtailment is transferred to the utility, and the total utility cost is:

$$\begin{aligned}
 Cost &= \sum_i [P_i \cdot \bar{f}_i(FOM_i)] \\
 &= P_1 \cdot \bar{f}_1(E_{loss}) + P_2 \cdot \bar{f}_2(f_{min_f}) + P_3 \cdot \bar{f}_3(\sigma)
 \end{aligned} \tag{2}$$

where P_i is the cost weighting for a 24 hour time period, and \bar{f}_i is the associated cost above the baseline value at the given penetration without the FW function, i.e., $\bar{f}_i = f_i(FOM) - f_i(FOM_0)$.

The price of electricity in Lanai was selected to be 0.448 \$/kWh based on the price of electricity for a single-phase residential homeowner on Lanai who uses 250 kWh of energy per month [45]. This corresponds to the incurred cost (due to lost revenue) of a residential homeowner curtailing to provide the frequency reserve. $P_1 = 1$ because E_{loss} represents an average 24 hour time period.

The f_{min_f} term was included to account for blackout costs. As of 2014, HECO implemented blocks of underfrequency load shedding (UFLS) with Stage 1 occurring at 58.7 Hz, Stage 2 at 58.5 Hz, and Stage 3 at 58 Hz [47], although, the UFLS relay trip points will be adjusted with higher penetration levels. The P_2 coefficient is the probability of the $N-1$ contingency occurring in a 24 hour period. Previously, Sandia analyzed HECO and MECO frequency data to determine the number and magnitude of over- and under-frequency events [48]. Using 2011 as a baseline, Maui Electric Company experienced 12 underfrequency events below 59.5 Hz (with 1 below 58.5 Hz), so P_2 was selected to be $12/365 = 0.033$ to represent the cost weighting (probability) of a grid disturbance for one day.

The cost of lost load can be calculated in different ways, but LBNL and DOE created a simple Interruption Cost Estimate (ICE) calculator to estimate the economic losses given the duration and severity of the blackout [49]. Here, it was assumed that 3,000 people on Lanai Island were residential customers, 200 were commercial and industrial, and the load was lost for 60 minutes. The percentage of the customers affected by the outage is linearized between 58.7 Hz Stage 1 UFLS and bulk collapse at 57 Hz—in part because PV frequency ride-through settings were recently widened to allow normal operation down to 57 Hz [50]. With these values and default ICE Hawaiian demographic information, the price for a complete blackout was calculated to be $P_b = \$253.5k$. Based on these assumptions,

$$f_2(f_{\min_f}) = \begin{cases} 0 & \text{for } f_{\min_f} > 58.7 \\ P_b \left(\frac{58.7 - f_{\min_f}}{1.7} \right) & \text{for } 57.0 \leq f_{\min_f} \leq 58.7 \\ P_b & \text{for } f_{\min_f} < 57.0 \end{cases} \quad (3)$$

Power plants experience additional wear when they are operated at larger ramp rates. The O&M costs for cycling the Lanai diesel generators is unknown, but previous work with coal and gas power plants indicate that the costs for doubling the ramp rate will increase the associated cycling costs by a factor of up to 10 [51]. When gensets operate with proportional droop control and there is an increase in the rate of variation of the grid frequency, the generator ramp rates will increase roughly proportionally and inflict a greater creep and fatigue damage. Assuming genset replacements costs are \$0.38/W and are incurred after 20,000 hrs (2.28 yrs) [52], the replacement costs for the 1.8 MW gensets on Lanai are \$822/day. Herein, it is assumed the severity of frequency deviation may be represented by frequency standard deviation, and it is assumed that there will be an additional 300% wear on the genset components when the grid frequency standard deviation doubles from the 20% baseline, such that:

$$f_3(\sigma) = P_{gen} \cdot C \left[1 + 3 \left(\frac{\sigma - \sigma_{0_20\%}}{\sigma_{0_20\%}} \right) \right] \quad (4)$$

where C is the replacement cost per watt and P_{gen} is the diesel power capacity interconnected to the system at different penetration levels.

Using the Latin Hypercube Sampling results, the influence of each parameter on the costs is depicted in Figure 21. As seen in the results, there are FW functions that result in cost savings for the utility in all penetration scenarios; specifically, there are minima in the curtailment values for each penetration level. The smaller deadbands produce slightly greater cost savings, but the droop has little influence on the total utility cost. As penetration increases, the utility would save more money from implementing the FW function, seen in the lowest LHS costs for each penetration in Table 4.

When comparing the results for each of the penetration level, it is clear that, at lower penetrations, the cost function favors deeper curtailment levels. This seems counter intuitive, but there is significantly less revenue loss at lower curtailment levels and FW

implementation extends the genset life by smoothing to the day-long MATLAB frequency results. At low penetrations, more diesel gensets are connected to the grid also; so, the curtailment is high to mitigate PV variability and provide headroom for control action and thus reduce generator wear. At higher penetration, the best curtailment value decreases since energy loss gets more expensive and is not offset by reduction in generator wear.

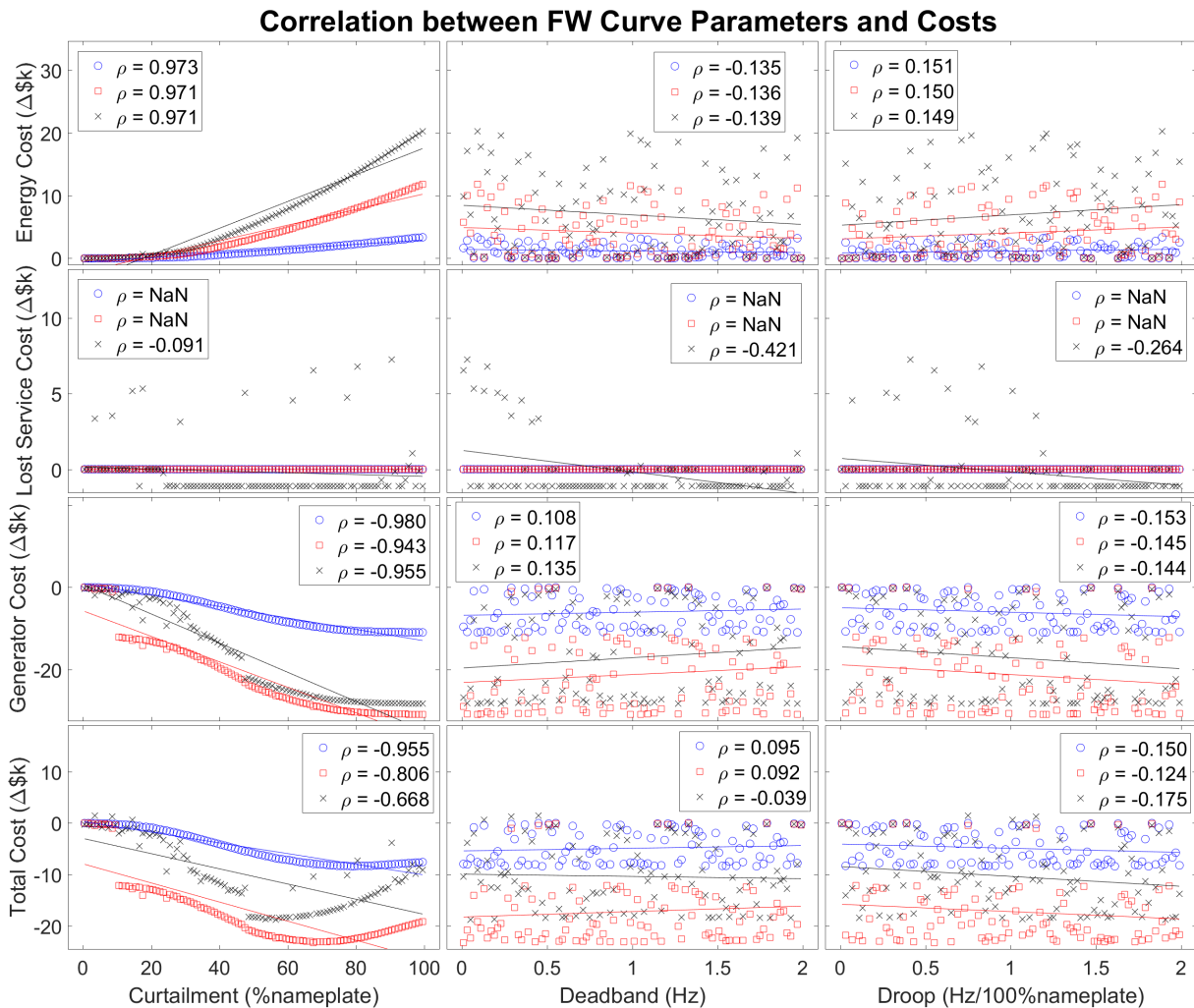


Figure 21. FW parameter influence on costs for 20% (blue), 70% (red) and 120% (black) penetration cases.

Optimization Method

The PSLF and MATLAB models were wrapped in an optimization tool to determine the FW curve that would provide the greatest savings to the utility. The problem is in the form of:

$$\min_{\mathbf{x}} f(\mathbf{x}) \text{ s.t. } \begin{cases} 0.002 \leq x_1 \leq 1.000 \\ 0.002 \leq x_2 \leq 2.000 \\ 0.002 \leq x_3 \leq 2.000 \end{cases}$$

$$\text{where } f(\mathbf{x}) = P_1 \cdot \bar{f}_1(E_{\text{loss}}(\mathbf{x})) + P_2 \cdot \bar{f}_2(f_{\text{min}_f}(\mathbf{x})) + P_3 \cdot \bar{f}_3(\sigma(\mathbf{x}))$$

where $\mathbf{x} = [x_1, x_2, x_3]$ and x_1 is the curtailment in p.u., x_2 is deadband in Hz, and x_3 is the droop in Hz/100%nameplate. The optimization routine was executed MATLAB, and the principle components are illustrated in Figure 21. Results of this development will be made available at the end of the performance period, November 30th.

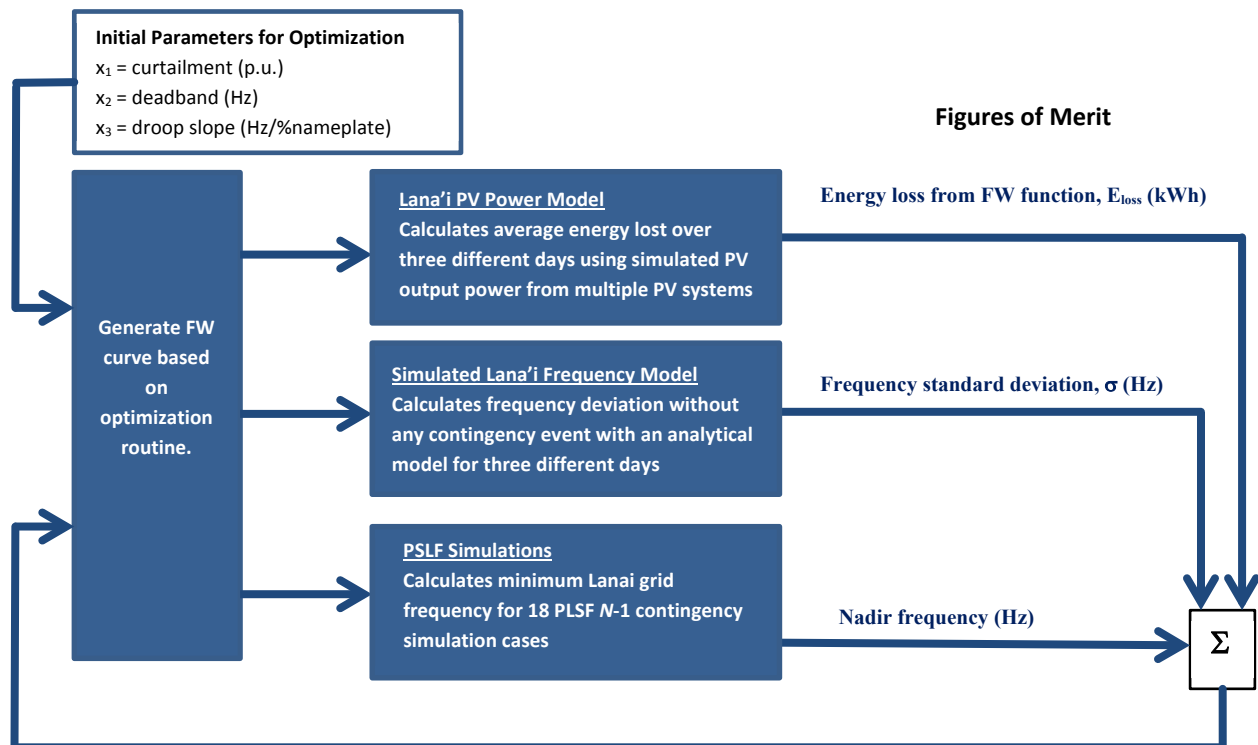


Figure 22: Optimization loop with MATLAB and PSLF models and associated figures of merit.

Initially, the optimization was attempted using the sequential quadratic programming (SQP) routine in MATLAB with the initial starting point near the best LHS result for each penetration level. Since there were no nonlinear equality or inequality constraints in the SQP optimization problem, the SQP algorithm approximated Newton's method to find the optimal FW curve. However, this technique failed to find a global minima and resulted in costs greater than the best LHS results after dozens of iterations. The SQP optimizer found a similar optimal curtailment level compared to the LHS, but it found much different deadband and droop values. This is due to weak cost correlations for these parameters and, possibly, from local minima in the fitness landscape with respect to these parameters. In order to improve the optimization results, a second optimization routine using the interior point method was also used to determine the optimal frequency watt curves. This time the starting point was selected to be the best LHS

result. As shown in Table 4, the interior point method resulted in slightly better solutions than the LHS data and the SQP method for the 70% and 120% penetration cases.

As can be seen in the results in Table 4, all the methods found similar curtailment values for each of the penetration levels, but there were discrepancies regarding the optimal deadband and droop values. When comparing the cost values, it is clear that both of the latter parameters are secondary effects and do not heavily influence the revenue from FW implementation. In some sense, this is excellent news for HECO and other utilities, because these low-sensitivity parameters do not need to be set precisely to see near-optimal returns from FW implementation.

Table 4: Best FW curves for LHS and optimization methods

Penetration	Technique	Curtailment (%)	Deadband (Hz)	Droop (Hz/100%nameplate)	Cost (Δ \$k)
20%	LHS	78.50	1.730	1.610	-8.35
	SQP	79.20	0.416	0.752	-8.35
	Interior Point	78.91	1.733	1.6221	-8.35
70%	LHS	67.50	0.010	0.551	-23.22
	SQP	67.67	0.033	1.027	-23.09
	Interior Point	67.11	0.002	0.416	-23.30
120%	LHS	56.50	0.050	1.910	-18.78
	SQP	56.56	1.611	1.529	-18.40
	Interior Point	47.70	0.042	0.004	-20.43

Hardware Experiments

To demonstrate the ability of frequency-watt implementation to mitigate frequency (generator speed) deviations and to help identify any practical considerations with implementation, experiments were performed at DETL. These experiments included a 225 kW diesel generator, a 24 kW inverter with frequency-watt capability, a 50 kW load and a 25 kW load. Four scenarios were considered: (a) the inverter operating with 100% of capacity with FW22 enabled, (b) the inverter operating with 100% of capacity with FW22 disabled, (c) the inverter operating at 50% of capacity with FW22 enabled, and (d) the inverter disconnected. Figure 23 shows the configuration of the experimental setup. Under all cases, the inverter DC input is sufficient to operate the inverter at rated power. Figure 24 shows the frequency response when load is stepped from 75 kW to 25 kW. In each case, generator speed increases rapidly after the load shed, but the peak frequency is lessened and the return to nominal speed is improved in the cases with frequency-Watt capability enabled.

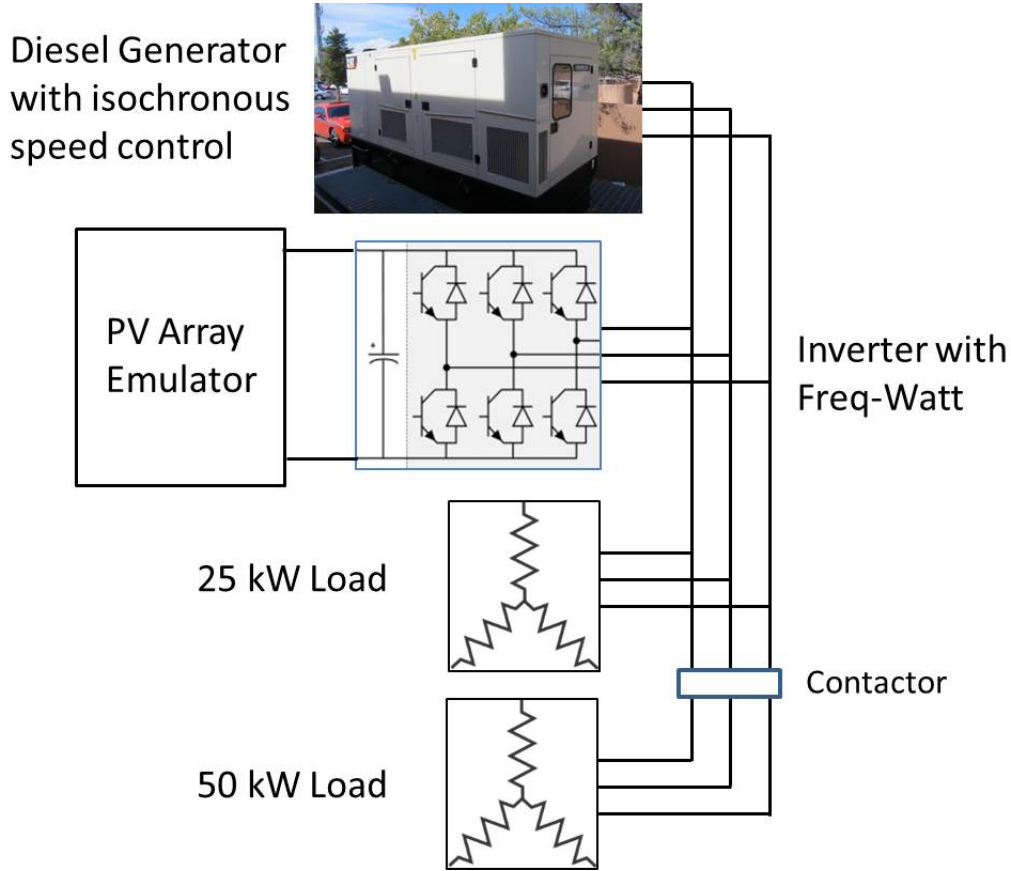


Figure 23: Experimental test setup including diesel generator, PV inverter equipped with frequency-watt capability and loads.

To quantitatively compare the frequency performance of each scenario, a figure of merit was chosen to represent overall frequency deviation with time:

$$f_e = \int_{t_0}^{t_f} (f(\tau) - f^*)^2 d\tau \quad (5)$$

where f_e is the integral square frequency error, expressed in $\text{Hz}^2 \cdot \text{s}$, or simply Hz ; f is the system frequency; f^* is the scheduled frequency; t_0 is the time that the step change in the load occurs; and t_s is the time at which the frequency transient settles. Another figure of merit is the amount of energy required from fossil fuels (in this case the diesel generator). These values are calculated over a 5-second time period, shown in Table 5. Therein, it is noted that the first case demonstrates the best frequency response and the second lowest consumption of fossil fuel energy for this experiment. The lowest fossil fuel consumption occurs in the second case (inverter at 100% of rated power, FW is disabled), where the inverter continues to operate 100% when the frequency surges from nominal during the step change in load.

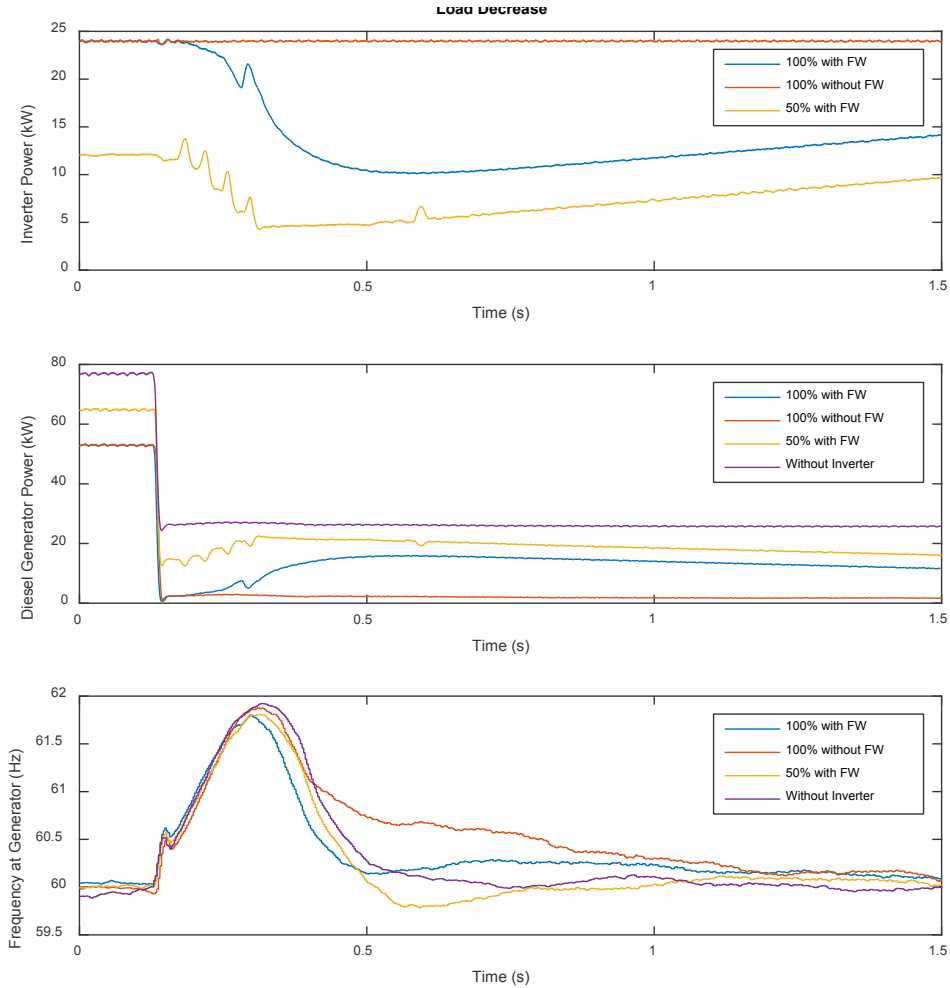


Figure 24: Response to a 75 kW to 25 kW step change in load

Table 5: Performance Comparison for a 75kW to 25kW step change in load

Time Horizon: 5 seconds	Frequency Error f_e	Diesel Energy (kJ)
Inverter at 100% capacity with FW22 Enabled	0.50993	36.666
Inverter at 100% capacity with FW22 Disabled	0.75181	11.026
Inverter at 50% capacity with FW22 enabled	0.51738	77.479
Diesel Generator with no inverter	0.61614	130.72

The inverter was able to quickly reduce its output power in accordance with the frequency-Watt settings and improve frequency/speed response during load shedding. However, an issue was identified for recovering to full power after the frequency falls. This is illustrated using only the inverter and grid simulation. In Figure 25, the frequency disturbance generated by the grid simulator, phase voltage of the inverter, phase current and DC link voltage are plotted. In particular, when the frequency rises from

60.0 Hz to 62.0 Hz, the output power drops immediately (within a couple cycles) to a value consistent with the FW22 settings. The AC voltage is steady and the DC link voltage is seen to rise as output power decreases, as expected. However, when the frequency recovers and returns to 60.0 Hz, the output power of the inverter is very sluggish to respond due to the maximum power point tracker time delay, recovering only 75% of the output power reduction in 3 seconds. This test was done twice with two different time delays between the up and down transitions. This time delay resulted in degraded frequency/speed recovery in experiments where load was added and the FW was enabled.

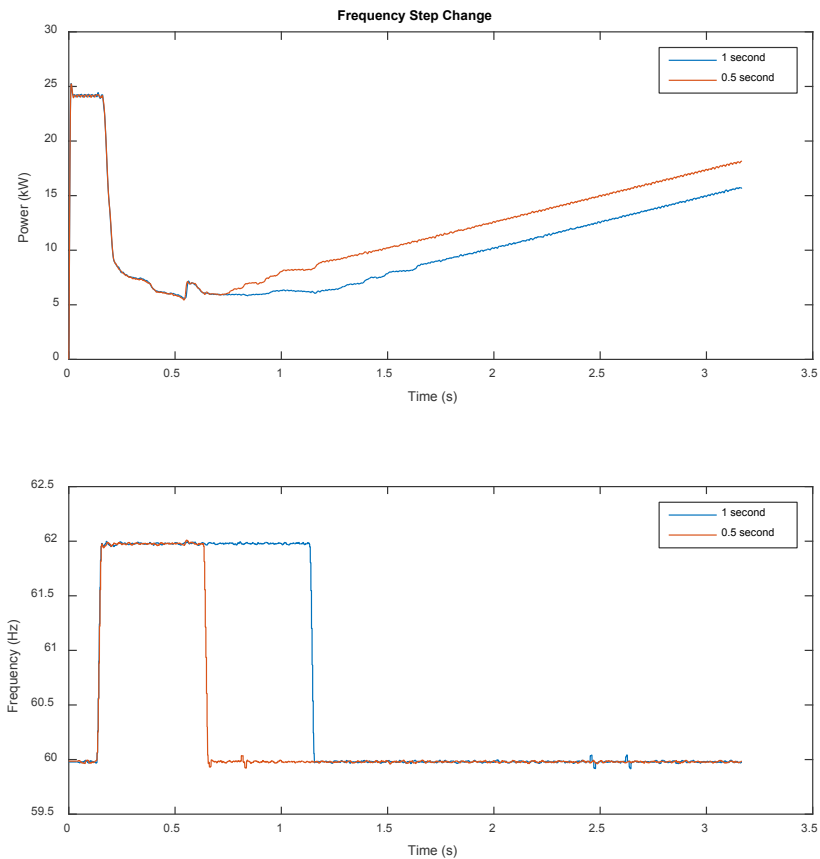


Figure 25: Inverter response to step changes in frequency

Significant Accomplishments and Conclusions:

In this work, we investigated the influence of the FW function on the Lanai, HI electricity grid in its current state with 20% PV penetration and in possible future configurations of 70% and 120% PV penetration. High-fidelity models were developed in MATLAB and PSLF to provide a complete representation of the island grid's response to PV variability and to faults and loss of generation in each configuration. These real-world models and scenarios were used in simulation efforts that clarified how the FW function affects the dynamics of the system, and they were used in optimization schemes to show how best to make money using the FW functions. The results showed that implementation of the FW function could immediately save HECO money even if they paid PV owners for the lost generation opportunity costs. Additional cost saving are available in the 70% and 120% PV penetration scenarios. This is a significant finding because it shows that the implementation of advanced grid functions does not only provide technical grid support, but is also economical when implemented with the proper settings. It is anticipated this will be the case for other regions and jurisdictions in the US and world, and the models and method of analysis can be extended to these areas to find the optimal FW settings; although the cost function could be expanded to include other expenses and the models for energy loss, lost load, and generator replacement costs could be improved.

Finally, this work included experimental investigation of the FW function providing frequency support in a microgrid testbed. The results showed promise but also revealed issues with inverter response time when frequency goes down and commanded output power increases. These results will be important for making manufacturers and utility stakeholders aware of this important issue and for informing response time metrics when updating function definitions.

Overall, the project successfully established a technique for finding the most economical FW curve for a region. This method can be adopted by utilities in CA, HI, and elsewhere in the world to pick desirable FW settings. As more inverters become compliant to IEC 61850-90-7 and are programmed with advanced grid support functions, they will increasingly become a major component of ancillary service strategy. Deployment of advanced interoperable inverters also opens the door for aggregations to provide ancillary services. These "virtual power plant" aggregations can be programmed to support grid frequency and voltage and also respond to grid disturbances, such as an $N-1$ contingency. In this project the VPP was able to smooth the grid frequency during non-contingency periods and also prevent bulk system collapse during an $N-1$ contingency by quickly injecting active power into the grid. In the future, VPPs can be constructed of diverse DER resources and designed to provide a range of services for utilities, ISOs, and RTOs. The economic incentive for utilities to do this was shown in this paper, but third party VPPs could also take advantage of this revenue stream by providing these capabilities and operating in ancillary service and energy markets.

Inventions, Patents, Publications, and Other Results:

The progress and findings of this one year project have been documented in two conference papers (one accepted and one in review) and one SAND report in development. In addition, the models developed in this effort were leveraged to foster collaboration with HECO on a Grid Modernization Lab Call (GMLC) category 1 proposal entitled "Grid Frequency Support from Inverter-based Resources"

Conference Papers:

Neely, J.; Johnson, J.; Delhotal, J.; Gonzalez, S.; "Evaluation of PV Frequency-Watt Function for Fast Frequency Reserves," Applied Power Electronics Conference and Exposition, APEC 2016. Thirty-first Annual IEEE; Long Beach, CA; 20-24 March 2016. (Accepted and submitted).

Johnson, J.; Neely, J.; Delhotal, J.; Lave, M.; "Photovoltaic Frequency-Watt Curve Design for Contingency Reserves," IEEE PVSC, Portland, OR; June 5-10, 2016. (In review)

SAND Report:

J. Neely, J. Johnson, M. Lave, S. Gonzalez, J. Delhotal, M. Baca; "Frequency-Watt Function Deployment for Fast Frequency Reserves from Aggregated PV Resources on Island Grids"; Sandia National Laboratories Technical Report; SAND2016-xxxxx; January 2016. (In development)

Path Forward:

There are four important next steps that should occur in order to properly leverage the results presented herein. They are given as:

- To ensure that inverters provide the fast response with both fall and rise in power, Sandia should work with inverter manufacturer(s) to mitigate the problem of slow power recovery in inverters that implement FW.
- In order to increase the benefit to the US, the models and analysis developed herein should be applied to larger power systems, such as other Hawaiian islands and/or to the western North American Power System (wNAPS). The PSLF PV models that input PV profiles and implement FW may be applied in Western Electric Coordinating Council (WECC) developed base cases to investigate FW implementation and optimization in high PV penetrated grids.
- Sandia and HECO should collaborate on the implementation of FW functions in the Lanai island grid or at least on larger testbeds to validate the results presented herein.
- Finally, the economic cost model should be validated and refined using more applicable economic data.

Sandia collaborated with NREL and HECO on the development of a GMLC category 1 proposal entitled “Grid Frequency Support from Inverter-based Resources.” If this opportunity is funded, Sandia will have the opportunity to continue this important work.

Funding Statement:

Sandia National Laboratories is a multi-program laboratory managed and operated by Sandia Corporation, a wholly owned subsidiary of Lockheed Martin Corporation, for the U.S. Department of Energy’s National Nuclear Security Administration under contract DE-AC04-94AL85000. This document was approved as SAND2015-xxxxx.

References:

- [1] J. Johnson, B. Schenkman, A. Ellis, J. Quiroz, C. Lenox; "Initial Operating Experience of the La Ola 1.2-MW Photovoltaic System"; Sandia National Laboratories Technical Report; SAND2011-8848; October 2011.
- [2] Johnson, R.; Johnson, L.; Nelson, L.; Lenox, C.; Stein, J., "Methods of integrating a high penetration photovoltaic power plant into a micro grid," *Photovoltaic Specialists Conference (PVSC), 2010 35th IEEE*, pp.289-294, 20-25 June 2010.
- [3] VDE Application Guide VDE-AR-N 4105, 1/08/2010: Generators in the low voltage distribution network. Application guide for generating plants' connection to and parallel operation with the low-voltage network.
- [4] IEC Technical Report IEC 61850-90-7, "Communication networks and systems for power utility automation—Part 90-7: Object models for power converters in distributed energy resources (DER) systems," Edition 1.0, Feb 2013.
- [5] Bründlinger, R.: *Grid Codes in Europe for Low and Medium Voltage*. 6th International Conference on Integration of Renewable and Distributed Energy Resources, Kyoto, Japan, 18 November, 2014.
- [6] R. Bründlinger "European Codes & Guidelines for the Application of Advanced Grid Support Functions of Inverters", Sandia/EPRI 2014 PV Systems Symposium - PV Distribution System Modeling Workshop, Santa Clara, CA, USA.
- [7] J. Johnson, S. Gonzalez, A. Ellis, "Sandia DER Interoperability Test Protocols; Relationship to Grid Codes and Standards", IEEE International Conference on Standards for Smart Grid Ecosystems, Bangalore, India. 6-7 Mar, 2014.
- [8] T. Hsu, Los Angeles Times, "Gov. Brown pushes 12-gigawatt clean-power goal," July 26, 2011.
- [9] J.F. Wiedman, et al., Interstate Renewable Energy Council, "12,000 MW of Renewable Distributed Generation by 2020," July 2012.
- [10] California Public Utilities Commission, "Recommendations for Updating the Technical Requirements for Inverters in Distributed Energy Resources, Smart Inverter Working Group Recommendations," Filed 7 February 2014.
- [11] J. Johnson, R. Bründlinger, C. Urrego, R. Alonso, "Collaborative Development Of Automated Advanced Interoperability Certification Test Protocols For PV Smart Grid Integration," EU PVSEC, Amsterdam, Netherlands, 22-26 Sept, 2014.
- [12] J. Johnson, B. Fox, "Automating the Sandia Advanced Interoperability Test Protocols," 40th IEEE PVSC, Denver, CO, 8-13 June, 2014.
- [13] J. Johnson S. Gonzalez, M.E. Ralph, A. Ellis, and R. Broderick, "Test Protocols for Advanced Inverter Interoperability Functions," Sandia Technical Report SAND2013- 9880 and SAND2013-9875, Nov. 2013.
- [14] J. C. Boemer, *et al* "Overview of German Grid Issues and Retrofit of Photovoltaic Power Plants in Germany for the Prevention of Frequency Stability Problems in

Abnormal System Conditions of the ENTSO-E Region Continental Europe,” 1st international workshop on integration of solar power into power systems, Denmark, October 2011.

- [15] http://www.pv-magazine.com/news/details/beitrag/germany-retrofits-200-000-pv-installations-to-meet-50-hz-requirement_100016243/
- [16] von Appen, J.; Braun, M.; Stetz, T.; Diwold, K.; Geibel, D., "Time in the Sun: The Challenge of High PV Penetration in the German Electric Grid," Power and Energy Magazine, IEEE , vol.11, no.2, pp.55,64, March-April 2013
- [17] J.T. Sullivan, CPUC Rulemaking 11-09-011 Agenda ID #13460, 13 November, 2014, Approved Dec. 2014.
- [18] IEEE Standard 1547a-2014, "IEEE Standard for Interconnecting Distributed Resources with Electric Power Systems - Amendment 1".
- [19] J.W. Smith, W. Sunderman, R. Dugan, B. Seal, "Smart inverter volt/var control functions for high penetration of PV on distribution systems," Power Systems Conference and Exposition (PSCE), 2011 IEEE/PES , pp.1,6, 20-23 March 2011.
- [20] M. Braun, T. Stetz, T. Reimann, B. Valov, and G. Arnold, "Optimal Reactive Power Supply in Distribution Networks—Technological and Economic Assessment for PV-Systems," in 24th European Photovoltaic Solar Energy Conference, Hamburg, Germany, 2009.
- [21] T. Stetz, W. Yan, and M. Braun, "Voltage Control in Distribution Systems with High Level PV-Penetration," in 25th European PV Solar Energy Conference, Valencia, Spain, 2010.
- [22] Seuss, J.; Reno, M.J.; Broderick, R.J.; Harley, R.G., "Evaluation of reactive power control capabilities of residential PV in an unbalanced distribution feeder," Photovoltaic Specialist Conference (PVSC), 2014 IEEE 40th , pp. 2094-2099, 8-13 June 2014.
- [23] Reno, M.J.; Coogan, K.; Grijalva, S.; Broderick, R.J.; Quiroz, J.E., "PV interconnection risk analysis through distribution system impact signatures and feeder zones," PES General Meeting | Conference & Exposition, 2014 IEEE , pp.1,5, 27-31 July 2014
- [24] Winter, C., Schwalbe, R., Heidl, M., Pruggler, W., Harnessing PV inverter controls for increased hosting capacities of smart low voltage grids: Recent results from Austrian research and demonstration projects. 4th International Workshop on Integration of Solar Power into Power Systems, Berlin, Germany, 10-11 Nov, 2014.
- [25] H. Bevrani, A. Ghosh, G. Ledwich, "Renewable energy sources and frequency regulation: survey and new perspectives, " Renewable Power Generation, IET, vol.4, no.5, pp.438-457, September 2010.
- [26] J. Aho, et al., "Tutorial of Wind Turbine Control for Supporting Grid Frequency through Active Power Control," 2012 American Control Conference, Montreal, Canada, June 27-29, 2012.

- [27] Oudalov, A.; Chartouni, D.; Ohler, C., "Optimizing a Battery Energy Storage System for Primary Frequency Control," *Power Systems, IEEE Transactions on*, vol.22, no.3, pp.1259,1266, Aug. 2007
- [28] J. Neely, R. Byrne, R. Elliott, J. Johnson, Structured Optimization For Parameter Selection Of Frequency-Watt Grid Support Functions For Wide-Area Damping, *International Journal of Distributed Energy Resources and Smart Grid*, Submitted Jan 2015.
- [29] Hoke, A.; Maksimovic, D., "Active power control of photovoltaic power systems," 2013 1st IEEE Conference on Technologies for Sustainability (SusTech), pp.70-77, 1-2 Aug. 2013.
- [30] Datta, M.; Senjyu, T.; Yona, A.; Funabashi, T.; Chul-Hwan Kim, "A Frequency-Control Approach by Photovoltaic Generator in a PV–Diesel Hybrid Power System," *Energy Conversion, IEEE Transactions on* , vol.26, no.2, pp.559,571, June 2011
- [31] P.P. Zarina, S. Mishra, P.C. Sekhar, Exploring frequency control capability of a PV system in a hybrid PV-rotating machine-without storage system, *International Journal of Electrical Power & Energy Systems*, Volume 60, September 2014, Pages 258-267.
- [32] Huanhai Xin; Yun Liu; Zhen Wang; Deqiang Gan; Taicheng Yang, "A New Frequency Regulation Strategy for Photovoltaic Systems Without Energy Storage," *Sustainable Energy, IEEE Transactions on* , vol.4, no.4, pp.985,993, Oct. 2013
- [33] Pappu, V.A.K.; Chowdhury, B.; Bhatt, R., "Implementing frequency regulation capability in a solar photovoltaic power plant," *North American Power Symposium (NAPS), 2010* , vol., no., pp.1,6, 26-28 Sept. 2010
- [34] Kakimoto, Naoto; Takayama, S.; Satoh, H.; Nakamura, K., "Power Modulation of Photovoltaic Generator for Frequency Control of Power System," *Energy Conversion, IEEE Transactions on* , vol.24, no.4, pp.943,949, Dec. 2009
- [35] "Lanai PV Interconnect Requirements Study"; Technical report from KEMA Inc.; June, 2008.
- [36] M. Lave, J. Kleissl, and J. S. Stein, "A Wavelet-Based Variability Model (WVM) for Solar PV Power Plants," *Sustainable Energy, IEEE Transactions on*, vol. PP, pp. 1-9, 2012.
- [37] S. Ong, C. Campbell, P. Denholm, R. Margolis, and G. Heath, "Land-Use Requirements for Solar Power Plants in the United States," National Renewable Energy Laboratory NREL/TP-6A20-56290, 2013
- [38] M. Lave, J. S. Stein, A. Ellis, C. W. Hansen, E. Nakashima, and Y. Miyamoto, "Ota City: Characterizing Output Variability from 553 Homes with Residential PV Systems on a Distribution Feeder," SAND2011-9011.
- [39] L. M. Hinkelman, "Differences between along-wind and cross-wind solar irradiance variability on small spatial scales," *Solar Energy*, vol. 88, pp. 192-203, 2013.

- [40] M. Lave and J. Kleissl, "Cloud speed impact on solar variability scaling – Application to the wavelet variability model," *Solar Energy*, vol. 91, pp. 11-21, 2013.
- [41] D. King, W. Boyson, and J. Kratochvil, "Photovoltaic Array Performance Model," SAND2004-3535, 2004.
- [42] D. King, S. Gonzalez, G. Galbraith, and W. Boyson, "Performance Model for Grid-Connected Photovoltaic Inverters," SAND2007-5036, Sandia National Laboratories, 2007.
- [43] M. Lave and J. Kleissl, "Testing a wavelet-based variability model (WVM) for solar PV power plants," in *IEEE Power and Energy Society General Meeting*, 2012.
- [44] M. Lave, J. Kleissl, and J. S. Stein, "A Wavelet-Based Variability Model (WVM) for Solar PV Power Plants," *IEEE Transactions on Sustainable Energy*, 2013.
- [45] M.D. McKay, R.J. Beckman, W.J. Conover, "A Comparison of Three Methods for Selecting Values of Input Variables in the Analysis of Output from a Computer Code", *Technometrics*, vol. 21, no.2, pp. 239–245, May 1979.
- [46] Maui Electric Company, Ltd. Lanai Division, Schedule "R" Residential Service, Decision and Order No. 31288, Filed May 31, 2013.
- [47] Maui Electric Company, Ltd., Maui Electric Power Supply Improvement Plan, Docket No. 2011-0092, Filed 26 Aug, 2014.
- [48] C.A. Silva Monroy, V.W. Loose, Hawaii Electric System Reliability, Sandia Technical Report, SAND2012-3862.
- [49] Interruption Cost Estimate (ICE) Calculator, accessed 23 Oct, 2015, available: <http://www.icecalculator.com/index.html>.
- [50] Hawaiian Electric Companies, Transient Over-Voltage and Frequency & Voltage Ride-Through Requirements for Inverter-Based Distributed Generation Projects, June 2015.
- [51] N. Kumar, P. Besuner, S. Lefton, D. Agan, and D. Hilleman, Power Plant Cycling Costs, NREL Report, NREL/SR-5500-55433, July 2012.
- [52] B. Kroposki, et al., Integrating High Levels of Renewables into the Lanai Electric Grid, Technical Report NREL/TP-5500-50994, June 2012.